1994AJ....107..751M

THE ASTRONOMICAL JOURNAL VOLUME 107, NUMBER 2 FEBRUARY 1994

EXTREME ULTRAVIOLET EXPLORER BRIGHT SOURCE LIST

ROGER F. MALINA, HERMAN L. MARSHALL,[1] BEHRAM ANTIA, CAROL A. CHRISTIAN, CARL A. DOBSON,[2] DAVID S. FINLEY, ANTONELLA FRUSCIONE, FORREST R. GIROUARD, ISABEL HAWKINS, PATRICK JELINSKY, JAMES W. LEWIS, J. S. MCDONALD,[3] KELLEY MCDONALD, ROBERT J. PATTERER,[4] VINCENT W. SABA, MARTIN M. SIRK, BRETT A. STROOZAS, JOHN V. VALLERGA, PETER W. VEDDER,[5] ALEXANDRIA WIERCIGROCH, AND STUART BOWYER[6]

Center for EUV Astrophysics, 2150 Kittredge Street, University of California, Berkeley, California 94720

Received 1993 September 29

ABSTRACT

Initial results from the analysis of the *Extreme Ultraviolet Explorer (EUVE)* all-sky survey (58–740 Å) and deep survey (67–364 Å) are presented through the *EUVE* Bright Source List (BSL). The BSL contains 356 confirmed extreme ultraviolet (EUV) point sources with supporting information, including positions, observed EUV count rates, and the identification of possible optical counterparts. One-hundred twenty-six sources have been detected longward of 200 Å.

1. INTRODUCTION

The primary scientific goal of the *Extreme Ultraviolet Explorer (EUVE)* mission (Bowyer & Malina 1991) was to conduct a photometric survey of the entire sky over the whole extreme ultraviolet (EUV) band, as well as to conduct a more sensitive survey along the ecliptic. *EUVE* was launched on 1992 June 7 on a USAF Delta II rocket and was placed in a circular orbit of 550 km altitude with an inclination of 28°. A six week long in-orbit checkout of the instrument showed that the four telescopes and seven detectors were working as planned. Over the following six months, two distinct surveys, the all-sky survey and the deep survey, were conducted with the four *EUVE* telescopes. The all-sky survey was carried out with four distinct filters that cover the wavelength region 58–740 Å and that are named by the materials of which they are composed: Lexan/B, Al/Ti/C, Ti/Sb/Al (or "Dagwood"), and Sn/SiO (or "tin"). Table 1 shows the ~10% instrument transmission wavelengths for all the bandpasses on the *EUVE* telescopes. From 1992 July 22 to 1993 January 21, the scanners were used to map about 80% of the sky with exposures varying from 400 s on the ecliptic equator to approximately 20 000 s at the ecliptic poles. Concurrently, the fourth telescope, the Deep Survey/Spectrometer (DS/S), was used to carry out the "deep" survey (more sensitive by a factor of ten) of a 2°×180° strip of the sky along the ecliptic in two filters (Lexan/B and Al/C) covering the wavelength region 67–364 Å.

The survey was interrupted on a monthly basis to conduct calibration pointings at selected bright EUV sources, resulting in survey gaps which had to be filled in during the second six months of the mission, from 1993 January to July. The data corresponding to the ~20% of the sky in the survey gaps are not included in this paper. Since the end of the survey phase of the mission, the three spectrometers that share the DS/S telescope are being pointed at targets chosen by guest observers selected by NASA. Details of the spectrometers and the *EUVE* Guest Observer (GO) program can be found in the *EUVE* GO Program Handbook, which is included in the NASA Research Announcement (1993).

In this paper we present the *EUVE* Bright Source List (BSL), which consists of bright EUV point sources detected during the 1992 July 22–1993 January 21 survey phase of the *EUVE* mission, as well as bright sources observed during the in-orbit calibration phase. Included in the list are source position, count rates for each wavelength band at which the source was detected, and a possible optical identification of the source. The list is not meant to be complete; rather it is the first release of the sources bright enough that their existence as EUV sources is not in doubt. The first *EUVE* catalogue is in preparation (Bowyer *et al.* 1993), which will present the analysis after reprocessing of the initial sky survey data.

2. THE *EUVE* INSTRUMENTS

The sky survey was conducted with three "scanning" telescopes, which were coaligned and pointed 90° away from the satellite spin axis during the survey. The satellite

[1]Currently at the Center for Space Research, MIT, 77 Massachusetts Ave., Cambridge, MA 02139.
[2]Currently with Dobson Software Innovations.
[3]Currently with the Department of Astronomy, San Diego State University, San Diego, CA 92182.
[4]Currently at Hughes STX, Goddard Space Flight Center.
[5]Currently at NASA Headquarters, Code SZ, Washington, DC 20546.
[6]Also with the Astronomy Department, University of California, Berkeley, CA 94720.

[7]The Wide Field Camera (WFC) on the *Röentgen Satellite (ROSAT)* has produced a list of EUV sources at the shortest EUV wavelengths (Pounds *et al.* 1993). The two filter bands employed in the WFC survey, *S1* (60–140 Å) and *S2* (110–200 Å), do not extend as far into the longer EUV wavelengths as do the *EUVE* filters, and they are less sensitive. The Lexan/B filter on the *EUVE* scanners is similar in bandpass to the *S1* filter of the WFC; the surveys in the Al/Ti/C, Dagwood, and tin filter bandpasses of *EUVE* are the first all-sky surveys made at these wavelengths.

 0004-6256/94/107(2)/751/14/$0.90 © 1994 Am. Astron. Soc.

© American Astronomical Society • Provided by the NASA Astrophysics Data System

1994AJ....107..751M

TABLE 1. 10% filter bandpasses.

Instrument	Filter	λ_{peak} (Å)	Bandpass (Å)
Deep survey	Lexan/B	91	67–178
	Al/C	171	157–364
Scanners A and B	Lexan/B	89	58–174
	Al/Ti/C	171	156–234
Scanner C	Ti/Sb/Al	405	345–605
	Sn/SiO	555	500–740

spun at three rotations per orbit so that, during an orbital night, the telescopes' scan path mapped a great circle on the sky. The DS/S telescope was aligned with the axis of rotation, which was kept pointed in the antiSun direction, and therefore advanced along the ecliptic at 0.986° per day. Two of the scanners (scanners A and B) are essentially duplicates of each other, incorporating a grazing incidence Wolter–Schwarzschild type-I telescope with gold electroplated mirror surfaces. They have a field of view of about 5° and a focal length of approximately 56 cm. The third scanner (scanner C) is a Wolter–Schwarzschild type-II telescope with the surface coated with electroless nickel. The field of view is slightly smaller (4°) and the focal length is 70 cm (Finley *et al.* 1988).

All seven detectors on *EUVE* consist of a *Z* stack of microchannel plates (MCPs) that are read out by a wedge-and-strip anode (Siegmund *et al.* 1986). The detectors are identical except for the photocathode deposited on the front surface to increase the quantum efficiency and the thin film filters used to define the bandpass. A magnesium fluoride photocathode was used on scanners A and B and the Deep Survey detectors, whereas the scanner C detector was operated without a photocathode (to decrease the sensitivity to the strong geocoronal line at 584 Å). The quantum efficiency of the detectors did not degrade significantly from the time of deposition of the photocathodes to the last calibration of the instrument on the ground, and there has not been any evidence of sensitivity variations of the instruments in orbit (with a few percent upper limit to any change).

The *EUVE* thin film filters were chosen to cover, as much as possible, the full EUV bandpass, while remaining spectrally distinct and reducing sensitivity to the strong geocoronal lines at 304, 584, and 1216 Å. The history of the filter development and optimization can be found in Vallerga *et al.* (1992), and the flight calibration results are given in Vedder *et al.* (1992). The filters above the scanner MCP detectors are broken into four quadrants, with scanners A and B both containing Lexan/B and Al/Ti/C. The longer wavelength filters required a different telescope with a larger grazing incidence angle to reduce the x-ray throughput since these filters were known to have substantial transmission in the soft x-rays (Finley *et al.* 1988). The Lexan/B filters have a low residual transmission at the UV wavelengths (>2300 Å) and though the solar-blind detectors' response is decreasing exponentially, there is still enough throughput ($\sim 10^{-10}$) that very bright FUV stars such as O and B stars can be detected. The instrument was carefully designed to limit detection of O and B stars to only the 100 brightest in the sky with $m_V \leqslant 5$. The Al/Ti/C filter also has a very slight soft x-ray leak to light with wavelengths shorter than 70 Å, evident in a slightly significant detection of the brightest soft x-ray source in the sky, Scorpius *X*-1.

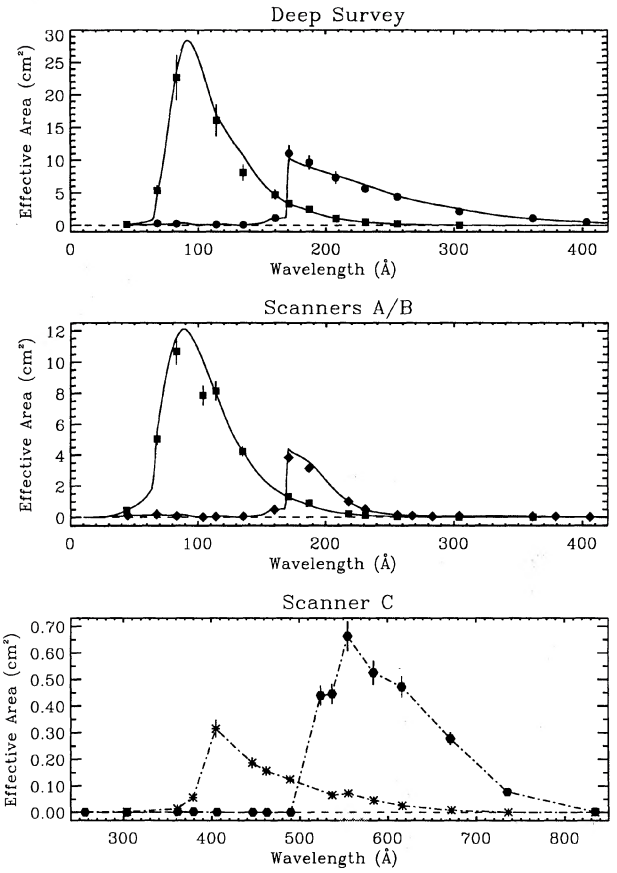

FIG. 1. *EUVE* effective areas for the Lexan/B (filled squares) and Al/C (filled circles) filters in the Deep Survey telescope, Lexan/B (filled squares) and Al/Ti/C (filled diamonds) filters in each one of the short wavelength scanners, and Dagwood (asterisks) and tin (filled hexagons) filters in Scanner C. The points mark the calibration values obtained prelaunch. For the Deep Survey and the short wavelength scanners, the solid line represents the best-fit model from in-flight measurements. No in-flight measurements are available yet for the scanner C filters.

The prelaunch calibration of *EUVE* was extensive. Absolute calibration traceable to primary standards provided by the National Institute of Standards and Technology (NIST) was performed on every instrument over the wavelength range of 23–2537 Å using monochromatic line sources of radiation (Welsh *et al.* 1990). Pencil beams were used to sample and map the response of the telescope aperture and the entire detector surface. These results were combined to give the effective area curves shown in Fig. 1. For the bandpasses that are on both scanners A and B, these effective areas represent the average of the two instrument effective areas (which differ by less than 10%). In-orbit calibration was carried out once a month to verify that there was no significant change in instrument performance.

© American Astronomical Society • Provided by the NASA Astrophysics Data System

1994AJ....107..751M

The background count rates for each detector are due to many sources, including intrinsic MCP background; geocoronal scattered solar radiation, predominantly 304 Å (He II), 584 Å (He I), and 1216 Å (H I); primary cosmic rays; low energy electrons in the Earth's radiation belts that can penetrate the magnetic brooms that cover the telescope aperture; and any possible cosmic diffuse EUV radiation. The Lexan/B bandpass background is dominated by the intrinsic background of the detectors due to the decay of K^{40} in the MCP glass. The Al/Ti/C and the Dagwood bandpasses include the 304 Å line, which thus dominates as a source of background, whereas the tin filter is strongly dominated by the 584 Å line. The background is variable owing to the spatial and temporal variability of the geocorona. The detectors are also strongly affected by passages through the South Atlantic Anomaly and by solar-induced geomagnetic storms, where the count rates can exceed 2000 cps, which causes an automatic shutdown of the detectors for health and safety reasons. However, the typical values of the background during a quiet orbit are very low, 1.7×10^{-4} counts s^{-1} sq arcmin^{-2} for the Lexan/B, 2.1×10^{-4} counts s^{-1} sq arcmin^{-2} for the Al/Ti/C band, 5.0×10^{-4} counts s^{-1} sq arcmin^{-2} for the Dagwood band, and 1.7×10^{-3} counts s^{-1} sq arcmin^{-2} for the Sn/SiO band. The total background is typically less than our telemetry bandwidth of $\sim$450 cps, so except for the brightest sources or high background events, corrections for deadtime due to the electronics or telemetry allocation are usually less than 10%.

The PSFs of the instruments are a strong function of the off-axis position of the source in the field of view because of the inherent off-axis aberrations the telescopes. However, for the survey, where most sources were sampled in the entire field of view, an average survey PSF can be determined for each bandpass. The half-energy radius for sources within 1.0° off axis is 1 arcmin for scanners A and B, and 0.5 arcmin for scanner C. An average PSF cannot be determined for the Deep Survey, as sources with different ecliptic latitudes sampled different parts of the detector field of view and were effectively observed with differing instrument PSFs.

3. THE BSL DEVELOPMENT

3.1 Science Data Products

The major science data products created by the *EUVE* data processing software are exposure maps, photon skymaps, and "pigeonholes" (for a detailed description of the *EUVE* software see Lewis *et al.* 1993; Antia 1993). Exposure maps (represented in Fig. 2 for each of the scanning and deep survey telescopes) contain information about the amount of time each region of the sky was surveyed. Raw photon skymaps represent the binned distribution of the EUV photons over the sky with a resolution of $\sim$1.3 arcmin/pixels. Pigeonholes are files containing detailed photon data for a circular area of sky (of $\sim$10 arcmin radius) centered on a selected position. The pigeonhole files also store additional precise information not included in the skymaps, such as the photons' arrival times and their

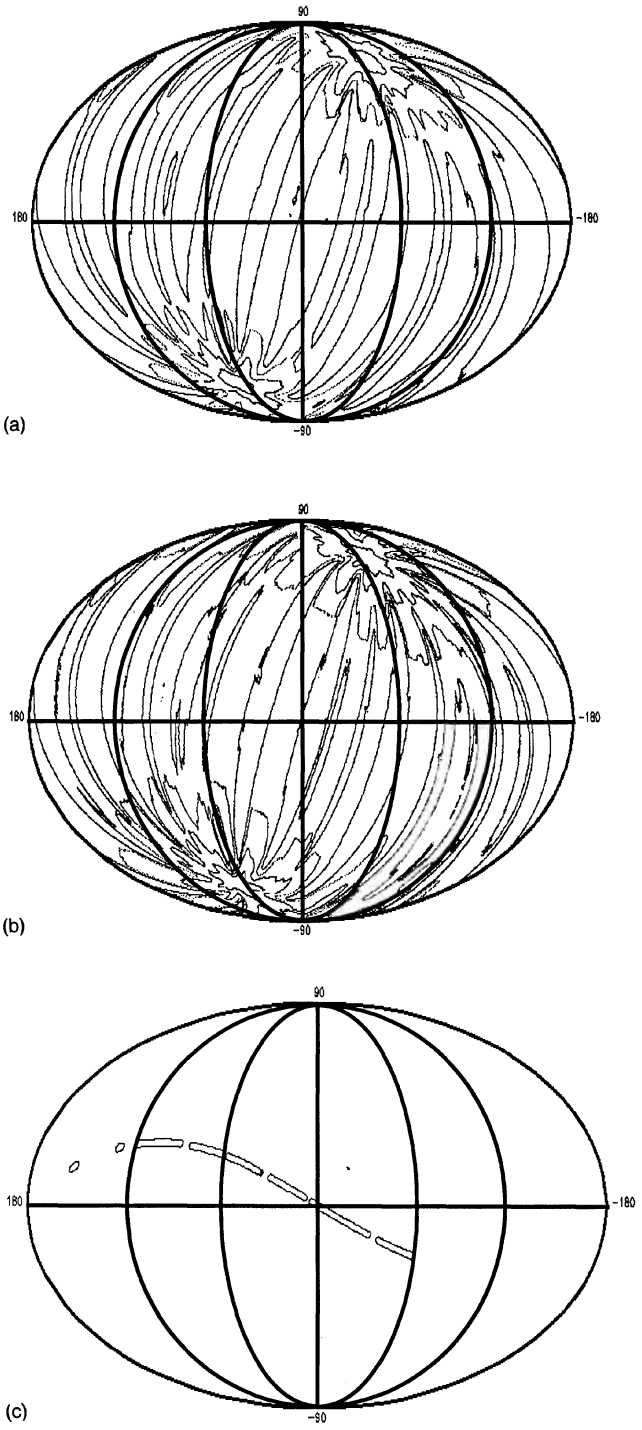

FIG. 2. Aitoff projections in equatorial coordinates (zero hours at the center and increasing toward the left) of the exposure maps for (a) the all-sky survey Lexan/B and Al/Ti/C filters; (b) Ti/Sb/Al and Sn/SiO filters; and (c) deep survey Lexan/B and Al/C filters. The figures show contour levels of equivalent exposure times for (a) 500, 1000, 2000, and 5000 s; and (b) 225, 500, 1000, and 2500 s where the highest contour for the all-sky survey exposure maps is the one near the ecliptic pole. The higher exposure around the ecliptic poles is a consequence of the survey geometry. In the deep survey exposure map, the contour shown is for 2500 s, and the exposure times reach up to 25 000 s within the contour. Gaps with no exposure result from the periods when the survey was stopped to carry out calibration.

© American Astronomical Society • Provided by the NASA Astrophysics Data System

1994AJ....107..751M

location on the detector, and also preserve a higher resolution of ~10 arcsec/pixel. Before the launch, a master pigeonhole catalogue containing ~6000 positions on the sky was compiled, corresponding to the best candidate EUV sources. Then detailed studies from the pigeonhole data for the most interesting objects was possible immediately after the first processing of the data, independent of the overall source detection process. The source detections were derived from analysis of the skymaps, whereas in most cases the pigeonholes, which allow more detailed study, were used in the source verification and in the count rate measurements.

3.2 All-Sky Survey Point Source Detection Approach

The scanner skymaps were searched for possible sources using a preliminary version of the *EUVE* source detection software (Lewis 1993). This code uses a two-pass method to produce the final list of detections. In the first pass, the skymaps are convolved with the appropriate PSF. The convolved data are treated as if they consisted of samples from a normal distribution; a threshold is applied to the peaks of the convolution, and significant deviations above the local background level are reported. The result of this pass is a list of "interesting" pixels, each 1.2×1.2 arcmin in size. The first-pass threshold is chosen so that real sources would be reported with very high probability while keeping the spurious detections to a manageable level. The second pass uses a more rigorous approach to examine each suspected source and calculate a more reliable detection statistic. The patch of sky around a suspected source is modeled as a locally flat background plus a source contribution folded through the PSF. The background level is estimated from a 15 to 24 arcmin annulus centered on the suspected source. A likelihood ratio test using this model is applied to the data, yielding a detection statistic distributed as χ^2. All sources with a detection statistic above ten form the *candidate* list. Because of the variable exposure time in different areas of the sky and the variations in the background, the minimum detectable flux of an object varies from area to area of the sky.

3.3 All-Sky Survey Point Source Measurement

The second stage in the compilation of the BSL consisted of a more critical analysis. The pigeonholes for each source in the BSL were analyzed with software based on a likelihood method developed independently of the source detection program (see Cruddace *et al.* 1988 for a similar application of this method to *ROSAT* x-ray data). The detailed time, position, and detector location data for all events in the pigeonholes were used to estimate simultaneously the source position, count rate, and background, assuming Poisson statistics. The model incorporates the detector vignetting map (which also includes blockage by the filter frame) and the telescope PSFs. The PSFs vary considerably with off-axis angle, so they have been computed for eight annuli in detector coordinates. As with the first-stage detection software, a likelihood statistic is formed and maximized for each source. The likelihood difference between the best value and the value obtained when the source count rate is fixed at zero is a measure of source existence and is distributed approximately as χ^2 with one degree of freedom. This existence test is more critical than the original detection statistic because more information is used: the PSFs vary with detector location and the event data are not binned as is the case for the skymaps. Therefore, although a source may appear to be significant to the detection program, it may be eliminated at this step.

The existence threshold was set at a value of 36, which for uniform Poisson background arrivals ought to yield a 10% probability of a single false source detection for the entire BSL spanning four independent all-sky maps.

The positions determined for bright, easily identified sources were compared to the higher accuracy optical positions in order to estimate systematic errors. Positions in the BSL are derived from the short wavelength telescope data (when available) for which a boresight offset has been estimated at 40 arcsec; all positions in the BSL have been corrected for this offset. Although some small systematic uncertainties still exist, all positions should be accurate to 60 arcsec at about 90% confidence. No boresight correction is yet available for the long wavelength telescope, and therefore the positions of the few sources detected only in the Dagwood or tin filters have not been corrected for this offset. The position of these sources should be accurate to ~90 arcsec at about 90% confidence.

The intensity of the sources was computed and the survey count rates for calibration sources were compared to their count rates calculated from the pointed calibration observation. In general, the calibration and survey count rates agreed to within 30%. Again, systematic uncertainties in the calibration data and the vignetting maps dominate for bright sources.

3.4 Deep Survey Sources

An objective detection algorithm for the deep survey is difficult because the PSF and exposure are strong functions of ecliptic latitude. The exposure can vary with ecliptic latitude by as much as a factor of 5 over 1°. Therefore, the sensitivity of the deep survey is not constant over ecliptic latitude, and sources more than 0.5° from the ecliptic have to be very bright in order to be detected. New algorithms for analyzing the deep survey data are being developed and will be used to produce the *EUVE* catalogue (Bowyer *et al.* 1993).

In order to include sources from the *EUVE* deep survey in the BSL, we used a simple (but subjective) visual detection process on the raw deep survey skymaps, binned at the 1.3 arcmin scale. Strong enhancements that had the spatial morphology of sources were included in the BSL if they had two or more adjacent pixels approximately 4σ above the surrounding local background. Preliminary count rates for the deep survey sources were derived from the deep survey skymap using a simple scheme wherein the source plus background counts are determined within a circle of ~2 arcmin radius around the source position, and the background is estimated in an annulus around the

© American Astronomical Society • Provided by the NASA Astrophysics Data System

1994AJ....107..751M

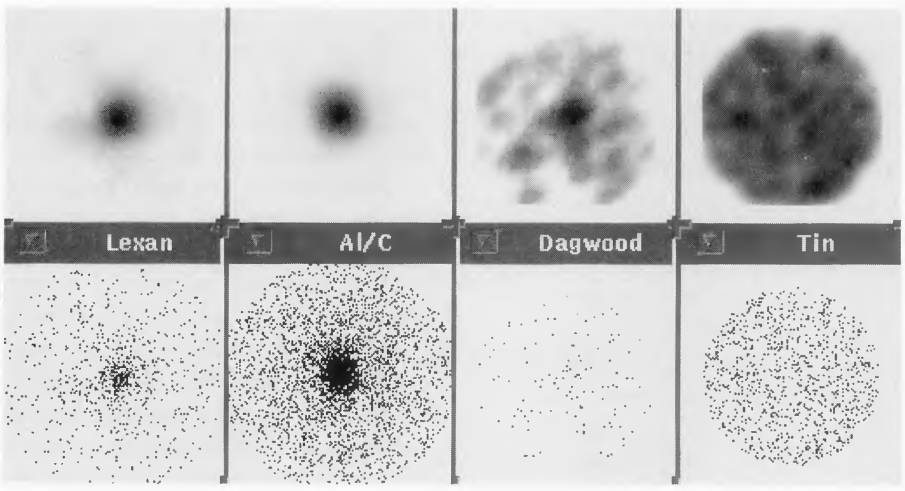

FIG. 3. Raw (bottom) and PSF-convolved (top) images for the pigeonhole corresponding to the white dwarf source *EUVE* J0623-37.6. The source is confirmed as detected in the Lexan/B, Al/Ti/C, and Dagwood filters from simultaneous visual inspection of the raw and convolved data.

source. For the sources far from the ecliptic and therefore farther off axis, larger apertures were used. Errors in the DS count rate should be within 50%.

3.5 BSL Selection Criteria

A major effort has been made to eliminate possible spurious sources from the BSL, and a *visual* verification test of the data was added to the source selection process as a further check, independent of the source detection and analysis software. Each candidate pigeonhole was convolved with the telescope PSF for each filter and independently examined by several researchers. Any sources with highly irregular images were set aside and removed from the BSL; further studies of these sources are under way, and the sources will be included in the *EUVE* catalogue if they are confirmed as definite detections. An example of the raw and PSF-convolved pigeonhole data that were examined is given in Fig. 3 for the source *EUVE* J0623-37.6.

As a result of the multiple-step process described above (detection in the skymaps, analysis of the pigeonholes, visual inspection), a source is included in the BSL *only if* the following criteria are satisfied *simultaneously*:

(a) The existence likelihood of the source (see Sec. *3.3*) is $\Delta S \geqslant 36$ in any single filter.

(b) No UV pinhole leak (see Sec. *3.6*) is revealed by a careful analysis of the scanning of the source in detector coordinates.

(c) The visual examination of the pigeonhole data, convolved with the telescope PSF, confirms the existence of the source, and the image shape is not anomalous.

In addition,

(d) sources with a detection likelihood of $10 \leqslant \Delta S \leqslant 36$ are included only if detailed examination of the source supported its detection via auxiliary data such as analysis of the light curve or positional coincidence with a known or candidate EUV or soft x-ray source.

(e) Sources observed during the calibration phase are also included. All these sources were detected in at least one filter with count rate uncertainties less than 15%.

(f) Sources detected visually from the deep survey skymaps are included if they satisfy the criteria explained in Sec. *3.4*.

The primary goal of the BSL (also in view of its use by prospective *EUVE* guest observers) was to be error free for the sources included. In this conservative process, a number of real sources may have been omitted (e.g., some 200 sources with significance between 10 and 36, with no clear counterpart and with no subsidiary studies to confirm the reality of the source, have been excluded from the BSL at this time). Readers should also note that some bright EUV sources do not appear in the BSL if they are located in the survey gaps. A later *EUVE* catalogue will be produced that is expected to contain more sources near the limit of detectability (Bowyer *et al.* 1993).

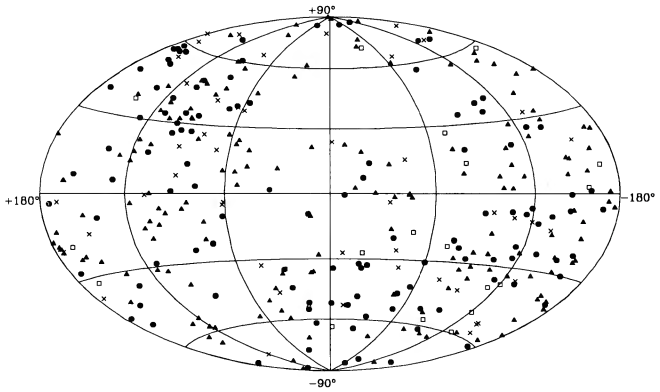

FIG. 4. Aitoff projections in galactic coordinates showing the location of the EUV sources in the BSL over the sky. White dwarf stars (filled circles), late-type stars (filled triangles), other classes of sources (crosses), and sources with no current possible identification (open squares) are plotted.

© American Astronomical Society • Provided by the NASA Astrophysics Data System

1994AJ....107..751M

Figure 4 is a map, in galactic coordinates, showing the locations of all the sources listed in the *EUVE* BSL.

3.6 Data Anomalies

There were two known filter anomalies affecting the data used for the BSL production. The first is due to a few tiny pinholes in the Lexan/B filter that allow non-EUV flux to be transmitted when a bright source is scanned across them. These pinhole leak sources were easily eliminated from the BSL in the visual verification process. The second problem is the known out-of-band residual transmission in the far UV in Lexan/B, which was inherent in the filter design and allowed UV detection of O and B stars brighter than $m_V \sim 5$. A calibration of these bright B stars is in progress to allow for estimating and subtracting the UV flux contribution. We have excluded all B stars from the BSL except for cases where additional, detailed analysis confirms the detection of an EUV signal. We have included in the BSL the A and B stars that were reported as extreme ultraviolet sources in the *ROSAT* WFC Bright Source Catalogue.

3.7 Diffuse and Extended Sources

Only pointlike sources have been included in this BSL. Any sources that appear significantly extended or diffuse have been omitted. Extended or diffuse EUV sources that have already been reported include the Moon (Gladstone *et al.* 1993), the Vela and Cygnus supernova remnants (Edelstein *et al.* 1993), and a cloud shadow (Bowyer *et al.* 1993). In addition, we have omitted extended sources detected by *EUVE* guest observers during GO pointings, but not detected during the sky survey; such sources include, e.g., Mars (Chakrabarti *et al.* 1993) and Jupiter (Moos *et al.* 1993).

4. THE BSL

Table 2 (this table is presented in its complete from in the ApJ/AJ CD-ROM Series, Vol. 2, 1994) contains information on the 356 sources that meet the selection criteria in Sec. *3.5*. The list includes all bright sources whose existence was established before 1993 April in the dataset obtained from 1992 June 7 to 1993 January 21. New sources continue to be found in the data and will be included in later releases of the *EUVE* catalogue. The table is ordered in right ascension, and is organized as follows.

Column 1. The *EUVE* source name as specified by the International Astronomical Union. Each source is identified by its J2000 coordinates in hours and minutes of right ascension and decimal degrees of declination. Errors in the preliminary BSL names (NASA Research Announcement 1993) for half a dozen sources have been corrected.

Columns 2 and 3. The right ascension (*hh:mm:ss*) and declination (*dd:mm:ss*) of the EUV source in J2000 coordinates. Positions should be accurate to 60 arcsec at about 90% confidence. Less accurate positions ($\sim$90 arcsec) are available at present for the few sources detected only in the Dagwood or Sn/SiO filters (due to unknown boresight errors), and for the sources detected in the deep survey skymaps. The distribution of the BSL sources over the sky is shown in Fig. 4.

Columns 4 and 5. The galactic longitude (l) and latitude (b) of the EUV source.

Columns 6–9. The count rate, in counts/kilosecond, for the sources detected in the scanners' Lexan/B, Al/Ti/C, Dagwood, and tin filters. The count rates have been calculated as explained in Sec. *3.3* and are accurate to within 50%, although there are occasional errors of a factor of 2 (see Sec. *3.3*). Count rates have been rounded to the nearest value in multiples of 10, except where the rounding would alter the count rate by more than 30%. Note that, although all BSL sources have $\Delta S \geqslant 10$, the list should *not* be considered complete at that level.

Count rates of calibration sources not scanned during the all-sky survey (because of gaps, etc.) were measured from the calibration data, on an orbit-by-orbit basis. The highest significant value [i.e., highest signal-to-noise ratio (SNR), and long exposure] has been quoted in the BSL. In cases when a calibration source was also scanned during the survey, the survey measurements have been quoted in the BSL. The detections by filter break down as follows: 327 sources in Lexan/B, 92 in Al/Ti/C, 17 in Dagwood, and 11 in tin. Table 3 lists BSL source detection by filter.

Columns 10 and 11. The count rate, in counts/kilosecond, for the sources detected in the Deep Survey Lexan/B (DSL) and Al/C (DSA) filters. The values are derived as explained in Sec. *3.4*, except for deep survey sources observed during the calibration phase, for which the count rate is derived as explained in the paragraph above. Some 39 sources were detected in the Deep Survey Lexan/B filter and 6 in the Al/C filter. (See Table 3.)

Columns 12 and 13. The possible optical counterpart of the EUV source and alternate name. The candidate counterparts come from a detailed search of astronomical catalogues, including the SIMBAD (Egret *et al.* 1991) and NED databases (Helou *et al.* 1991). We choose the possible counterparts among the sources most likely to emit EUV radiation, e.g., white dwarfs, active late-type stars, cataclysmic variables, and active extragalactic objects in low hydrogen column density directions ($\lesssim 2 \times 10^{20}$ cm^{-2}). All counterparts lie within 1.5 arcmin of the *EUVE* source position, except for the deep survey sources, where the most likely candidate within 3 arcmin of the detected location is listed. (The rate of coincidental identification at 3 arcmin for the deep survey sources was tested by searching for candidates around random positions: only 1 "false" object out of 39, equal to the total number of deep survey sources, had a plausible counterpart.)

No detailed nomenclature is given in general for different components of a same system (e.g., binary systems) and the notation "NOID" is used for currently unidentified sources. For the purpose of this BSL, we chose the most likely identification in case the EUV source had more than one possible optical counterpart: follow-up spectroscopy and photometry are in progress to identify all the NOID sources and to confirm the other identifications. A

© American Astronomical Society • Provided by the NASA Astrophysics Data System

1994AJ....107..751M

more detailed description of the optical identification process is given in Christian *et al.* (1993).

Column 14. The source type or spectral type of the optical candidate for the EUV source. Spectral types generally come from the SIMBAD database and follow the SIMBAD spectral type coding (see Appendix D of the SIMBAD User's Guide and Reference Manual). Extragalactic source types are from NED. Some of the white dwarf spectral types were provided by Finley (1993). The notation "CSPN" indicates the central star of a planetary nebula, "XRB" an x-ray binary system, and "LMXB" a low mass

TABLE 2. The EUV bright source list.†

EUVE Name	R.A. (J2000)	Decl. (J2000)	l	b	Lex c/ks	AlC c/ks	Dag c/ks	Tin c/ks	DSL c/ks	DSA c/ks	Possible ID	Other Name	Source Type	Mag	WFC Name	Notes
(1)	(2)	(3)	(4)	(5)	(6)	(7)	(8)	(9)	(10)	(11)	(12)	(13)	(14)	(15)	(16)	(17)
EUVE J0006+58.4	00 06 13	+58 25 46	117.0	−3.9	20	—	—	—	—	—	V640 Cas	HD123	G5V	5.93	—	—
EUVE J0007+33.3	00 07 33	+33 18 01	112.5	−28.7	200	—	—	—	—	—	WD0004+330	GD2	DA1	13.82	RE0007+331	B, I1
EUVE J0018+30.9	00 18 20	+30 57 12	114.6	−31.4	70	—	—	—	—	—	HD1405	SAO53799	G5	8.6	—	—
EUVE J0030−63.4	00 30 01	−63 25 24	307.0	−53.5	670	50	—	—	—	—	MCT0027−6341	—	DA	15.2	RE0029−632	B, I1
EUVE J0030−48.2	00 30 32	−48 13 09	312.5	−68.5	50	40	—	—	—	—	HD2726	HR120	F2V	5.69	—	—
EUVE J0042+04.1	00 42 24	+04 10 36	118.6	−58.6	—	—	—	—	9	—	HD3972	SAO109392	F8V	7.58	—	A, G
EUVE J0043−17.9	00 43 36	−17 59 25	111.3	−80.7	50	—	—	—	—	—	β Cet	HD4128	K0III	2.04	RE0043−175	—
EUVE J0044+09.5	00 44 02	+09 32 29	119.9	−53.3	40	—	—	—	—	—	BD+08 102	AG+09 55	G	10.0	RE0044+093	—
EUVE J0047−11.8	00 47 04	−11 52 06	118.9	−74.7	100	—	—	—	—	—	NGC246	PHL829	CSPN	11.78	RE0047−115	—
EUVE J0048+05.3	00 48 15	+05 18 45	121.5	−57.6	—	—	—	—	34	—	HD4628	HR222	K2V	5.75	—	A, G
EUVE J0053−74.6	00 53 13	−74 40 00	302.8	−42.5	30	—	—	—	—	—	CF Tuc	HD5303	G3:V+WD	7.60	RE0053−743	—
EUVE J0053−33.0	00 53 18	−33 00 12	299.1	−84.1	1650	840	—	160	—	—	WD0050−332	GD659	DA1	13.38	RE0053−325	B, E8, I1
EUVE J0057−22.3	00 57 21	−22 22 34	139.0	−85.1	60	—	—	—	—	—	KUV00549−2239	—	WD	15.0	—	—
EUVE J0106−22.8	01 06 47	−22 51 15	162.9	−84.5	60	—	—	—	—	—	HD6628	SAO166806	G5V	7.68	RE0106−225	—
EUVE J0108−35.5	01 08 23	−35 34 52	280.8	−80.8	70	—	—	—	—	—	WD0106−358	GD683	DA2	15.8	RE0108−353	I1
EUVE J0113+07.5	01 13 33	+07 34 34	132.5	−54.9	—	—	—	—	19	—	ζ Psc B	HD7345	F7V	6.32	—	A, G
EUVE J0116−02.5	01 16 38	−02 30 51	137.8	−64.7	70	—	—	—	—	—	AY Cet	HD7672	G5IIIe	5.41	RE0116−022	—
EUVE J0122+00.7	01 22 50	+00 42 45	139.4	−61.2	30	—	—	—	—	—	HD8358	BI Cet	G0	8.29	RE0122+004	—
EUVE J0134−16.1	01 34 24	−16 07 18	167.3	−75.2	660	150	—	—	—	—	WD0131−164	GD984	DA1	13.8	RE0134−160	I1
EUVE J0135−29.9	01 35 03	−29 54 43	231.7	−80.0	60	—	—	—	—	—	HD9770	SAO193189	K3V	7.09	RE0135−295	—
EUVE J0138+25.3	01 38 52	+25 23 26	136.2	−36.3	90	—	—	—	—	—	WD0136+251	PG0136+251	DA1p	15.9	RE0138+252	I1
EUVE J0138−17.9	01 38 58	−17 56 48	175.4	−75.7	140	—	—	—	—	—	UV Cet	GJ65A/B	M5.5V:e	12.52	RE0139−175	D3, E4
EUVE J0148−25.5	01 48 12	−25 33 20	209.1	−77.2	20	—	—	—	—	—	GD1401	BPM47349	DA1	14.3	RE0148−253	I1
EUVE J0150+67.6	01 50 59	+67 40 30	128.6	5.5	60	—	—	—	—	—	WD0147+674	GD421	DA1	14.42	RE0151+673	I1
EUVE J0153+29.5	01 53 04	+29 35 14	138.6	−31.4	40	30	—	—	—	—	α Tri	HD11443	F6IV	3.41	—	—
EUVE J0155−51.6	01 55 56	−51 36 48	280.9	−62.7	50	—	—	—	—	—	χ Eri	HD11937	G8IIIbCNvar...	3.70	—	—
EUVE J0204+77.2	02 04 51	+77 16 16	127.1	15.0	40	—	—	—	—	—	47 Cas	HD12230	F0Vn	5.27	RE0205+771	—
EUVE J0218+14.6	02 18 46	+14 36 43	152.5	−43.2	50	—	—	—	222	—	WD0216+143	PG0216+144	DA1	14.53	—	G, I1
EUVE J0228−61.3	02 28 22	−61 18 54	284.2	−52.1	1000	110	—	—	—	—	HD15638	SAO248569	F3IV/V+DA	8.8	RE0228−611	—
EUVE J0230−47.9	02 30 55	−47 55 56	266.6	−61.6	80	60	—	—	—	—	LB1628	JL295	DA1	14.53	RE0230−475	I1
EUVE J0232+15.0	02 32 56	+15 02 19	156.3	−41.2	—	—	—	—	61	—	29 Ari	HD15814	F8V	6.00	—	A, G
EUVE J0234−43.8	02 34 23	−43 48 03	258.5	−63.4	120	—	—	—	—	—	CC Eri	HD16157	K7Ve	8.70	RE0234−434	—
EUVE J0235+03.7	02 35 04	+03 44 35	165.9	−50.3	1060	5220	650	340	4590*	—	Feige 24	WD0232+035	DAZ1	12.40	RE0235+034	B, I1
EUVE J0237−12.3	02 37 26	−12 21 42	187.4	−61.1	170	90	—	—	—	—	PHL1400	—	DA1	15.1	RE0237−122	I1
EUVE J0239−58.1	02 39 00	−58 11 31	279.2	−53.7	50	—	—	—	—	—	GJ1049	CPD−58 223	M0Ve	9.65	—	—
EUVE J0239+50.0	02 39 45	+50 03 18	140.2	−9.2	40	—	—	—	—	—	RE0239+500	—	DA1	15.6	RE0239+500	—
EUVE J0241−52.9	02 41 41	−52 59 30	272.1	−57.0	40	—	—	—	—	—	NOID	—	—	—	—	—
EUVE J0243−37.9	02 43 22	−37 56 09	244.7	−64.2	90	—	—	—	—	—	UX For	HD17084	G6V+...	8.1	RE0243−375	—
EUVE J0248+31.1	02 48 44	+31 07 00	150.6	−25.4	110	—	—	—	—	—	VY Ari	HD17433	G9Ve	6.76	RE0248+310	—
EUVE J0252−12.7	02 52 32	−12 46 37	192.1	−58.3	60	—	—	—	—	—	HD17925	HR857	K1V	6.00	—	—
EUVE J0254−05.3	02 54 38	−05 19 16	181.8	−53.5	140	30	—	—	—	—	HD18131	SAO130180	K0	7.2	RE0254−051	—
EUVE J0304+02.9	03 04 30	+02 57 23	175.0	−46.0	30	—	—	—	—	—	Feige 31	WD0302+027	DA	14.88	—	I1
EUVE J0308+40.9	03 08 11	+40 57 09	149.0	−14.9	200	—	—	—	—	—	β Per	HD19356	B8V	2.12	RE0308+405	H
EUVE J0311−31.8	03 11 31	−31 52 21	230.3	−59.3	70	—	—	—	—	—	NOID	—	—	—	—	—
EUVE J0312−28.9	03 12 08	−28 59 44	224.7	−59.0	130	—	—	—	—	—	α For	HD20010	F8IV	3.85	—	—
EUVE J0314−22.5	03 14 12	−22 35 20	212.9	−57.4	390	—	—	—	—	—	EF Eri	H0311−22.7	CVAM	13.7	RE0314−223	—
EUVE J0317−85.5	03 17 32	−85 32 24	299.8	−30.7	90	30	—	—	—	—	LB9802	—	DA	13.9	RE0317−853	I2
EUVE J0318+18.4	03 18 15	+18 24 23	165.0	−32.2	—	—	—	—	9	—	NOID	—	—	—	—	A, G
EUVE J0322−53.7	03 22 17	−53 45 34	267.3	−51.6	160	50	—	—	—	—	LB1663	1E0320.9−5355	DA	14.9	RE0322−534	B, I1
EUVE J0326+28.7	03 26 32	+28 43 50	159.5	−22.9	440	—	—	—	—	—	UX Ari	HD21242	G5IV	6.47	RE0326+284	—
EUVE J0327+09.7	03 27 08	+09 44 16	174.0	−37.2	40	—	—	—	—	—	ξ Tau	HD21364	B9Vn	3.73	RE0327+094	H
EUVE J0332−09.4	03 32 56	−09 27 09	195.8	−48.0	110	80	—	—	—	—	ϵ Eri	HD22049	K2V	3.73	RE0332−092	—
EUVE J0333+46.2	03 33 10	+46 14 57	149.9	−8.0	20	—	—	—	—	—	HD21845	SAO38935	K2	8.5	RE0333+461	—
EUVE J0333−25.8	03 33 13	−25 51 56	220.4	−53.9	140	—	—	—	—	—	NGC1360	PHL1556	CSPN	11.33	—	—
EUVE J0335−25.7	03 35 28	−25 43 54	220.3	−53.4	1090	50	—	—	—	—	UZ For	—	CVAM	18.2	—	—
EUVE J0336+00.5	03 36 46	+00 35 59	184.9	−41.6	570	—	—	—	1020*	—	V711 Tau	HD22468	G9V	5.71	RE0336+003	B
EUVE J0336+00.4	03 36 55	+00 24 50	185.1	−41.7	—	—	—	—	110*	—	10 Tau	HD22484	F9IV−V	4.28	—	C
EUVE J0337+26.0	03 37 06	+26 00 14	163.4	−23.6	90	—	—	—	—	—	V837 Tau	HD22403	G2V...	8.1	RE0337+255	—
EUVE J0348−00.9	03 48 48	−00 58 00	188.9	−40.1	440	290	190	350	—	—	WD0346−011	GD50	DA1	14.05	RE0348−005	I1
EUVE J0350+17.2	03 50 21	+17 15 31	172.5	−27.9	730	550	—	—	—	—	V471 Tau	BD+16 516	K0+DA2	9.7	RE0350+171	I1
EUVE J0355−01.7	03 55 18	−01 43 16	190.9	−39.2	40	—	—	—	—	—	HD24681	SAO130820	G5	9.5	—	—
EUVE J0356−36.6	03 56 33	−36 40 28	238.6	−50.0	150	—	—	40	—	—	NOID	—	—	—	—	—
EUVE J0357+28.6	03 57 05	+28 38 02	165.1	−18.7	50	—	—	—	—	—	RE0357+283	—	—	13.0	RE0357+283	—
EUVE J0409−71.2	04 09 17	−71 17 59	284.9	−38.1	15	—	—	—	—	—	VW Hyi	HV8028	CVDN	8.50	RE0408−711	—
EUVE J0409−07.8	04 09 39	−07 52 40	200.1	−39.4	100	—	—	—	—	—	EI Eri	HD26337	G5IV	7.08	RE0409−075	—
EUVE J0414−62.4	04 14 22	−62 28 15	274.3	−41.7	15	—	—	—	—	—	α Ret	HD27256	G8II−III	3.35	—	—
EUVE J0415−07.6	04 15 21	−07 38 26	200.8	−38.0	40	—	—	—	—	—	40 Eri	HD26965	K1V	4.41	RE0415−073	F
EUVE J0418+21.5	04 18 22	+21 34 49	174.0	−20.2	—	—	—	—	16	—	51 Tau	HD27176	F0V	5.60	—	A, G
EUVE J0419+21.7	04 19 37	+21 45 07	174.1	−19.8	—	—	—	—	23	—	56 Tau	HD27309	A0sp...	5.38	—	A, G
EUVE J0424+21.7	04 24 17	+21 44 20	174.8	−19.0	—	—	—	—	20	—	HD27808	SAO76593	F8V	7.14	—	A, G
EUVE J0426−57.2	04 26 01	−57 12 10	267.0	−42.0	50	—	—	—	—	—	1H0419−577	—	AGN	—	—	D1
EUVE J0426+21.4	04 26 19	+21 27 37	175.4	−18.9	—	—	—	—	4	—	HD28033	SAO76609	F8	7.38	—	A, G
EUVE J0427+74.1	04 27 36	+74 06 44	136.3	17.2	150	—	—	—	—	—	RE0427+740	—	DA1	15.5	RE0427+740	I1
EUVE J0429+21.9	04 29 02	+21 54 18	175.5	−18.1	—	—	—	—	19	—	HD28343	SAO76626	K7V	8.27	—	A, G
EUVE J0436+27.1	04 36 50	+27 07 38	172.5	−13.4	60	—	—	—	—	—	V833 Tau	HD283750	K2	8.42	RE0436+270	D3, E4
EUVE J0441+20.9	04 41 20	+20 54 39	178.2	−16.5	130	—	—	—	—	—	V834 Tau	HD29697	K3V	7.98	RE0441+205	—
EUVE J0443−03.7	04 43 06	−03 46 54	200.7	−30.1	130	—	—	—	—	—	RE0443−034	—	DA1	16.0	RE0443−034	I1
EUVE J0453−42.2	04 53 27	−42 12 21	246.7	−39.1	40	—	—	—	—	—	RE0453−421	—	—	—	RE0453−421	—
EUVE J0457−28.1	04 57 09	−28 07 35	229.3	−36.2	800	5760	860	520	—	—	MCT0455−2812	—	DA1	14.2	RE0457−280	B, I1
EUVE J0458+00.4	04 58 15	+00 26 57	198.7	−24.7	40	—	—	—	—	—	V1198 Ori	HD31738	G5	7.10	RE0458+002	—
EUVE J0459+37.8	04 59 33	+37 51 22	167.2	−2.9	40	—	—	—	—	—	BD+37 1005	HD31647	A1V	4.95	RE0459+375	H
EUVE J0459+01.7	04 59 34	+01 46 22	197.6	−23.8	30	—	—	—	—	—	V1005 Ori	GJ182	M1Ve	10.05	—	D3, E4
EUVE J0459−10.2	04 59 50	−10 15 52	209.6	−29.4	140	40	—	—	—	—	HD32008	HR1608	G4V	5.38	RE0459−101	—
EUVE J0500−36.3	05 00 04	−36 23 32	239.5	−37.2	30	—	—	—	—	—	RE0500−362	—	—	—	RE0500−362	—
EUVE J0503−28.8	05 03 51	−28 52 49	230.6	−34.9	50	540	1160	1140	—	—	MCT0501−2858	—	DOZ1	13.9	RE0503−285	B
EUVE J0505−57.4	05 05 25	−57 26 51	266.0	−36.7	50	—	—	—	—	—	ζ Dor	HD33262	F7V	4.72	RE0505−572	—
EUVE J0505+52.8	05 05 28	+52 49 42	156.0	7.1	2360	12360	2210	1490	11010*	—	G191−B2B	WD0501+527	DAZ1	11.78	RE0505+524	B, I1
EUVE J0506−21.5	05 06 47	−21 34 41	222.5	−32.2	50	—	—	—	—	—	BD−21 1074	—	M2V	10.1	RE0506−213	—

© American Astronomical Society • Provided by the NASA Astrophysics Data System

1994AJ....107..751M

TABLE 2. (continued)

EUVE Name	R.A. (J2000)	Decl. (J2000)	l	b	Lex c/ks	AIC c/ks	Dag c/ks	Tin c/ks	DSL c/ks	DSA c/ks	Possible ID	Other Name	Source Type	Mag	WFC Name	Notes
(1)	(2)	(3)	(4)	(5)	(6)	(7)	(8)	(9)	(10)	(11)	(12)	(13)	(14)	(15)	(16)	(17)
EUVE J0512−00.7	05 12 07	−00 42 06	201.7	−22.3	330	80	—	—	—	—	RE0512−004	—	DA	13.9	RE0512−004	I1
EUVE J0512−41.7	05 12 24	−41 44 46	246.5	−35.6	180	—	—	—	—	—	RE0512−414	—	DA:	16.5	RE0512−414	—
EUVE J0515+32.6	05 15 23	+32 40 54	173.3	−3.4	1900	640	—	—	—	—	HD33959C	SAO57798	A2+DA	7.95	RE0515+324	—
EUVE J0516+45.9	05 16 42	+45 59 37	162.6	4.6	390	130	—	—	1090*	—	α Aur	HD34029	G5IIIe+...	0.08	RE0516+455	B
EUVE J0517+45.8	05 17 21	+45 50 42	162.8	4.6	—	—	—	—	30*	—	GJ195.0A	—	M2V	10.16	—	C
EUVE J0517−35.3	05 17 26	−35 21 15	239.0	−33.6	40	—	—	—	—	—	RE0517−352	—	MVe	13.0	RE0517−352	—
EUVE J0521−10.4	05 21 18	−10 28 42	212.3	−24.7	140	90	—	—	—	—	RE0521−102	—	DA1	16.0	RE0521−102	I1
EUVE J0527−11.8	05 27 05	−11 53 29	214.4	−24.0	100	—	—	—	—	—	HD35850	HR1817	F7V:	6.35	RE0527−115	—
EUVE J0528−65.4	05 28 41	−65 27 01	275.3	−33.1	170	30	—	—	—	—	AB Dor	HD36705	K1IIIp...	6.83	RE0528−652	—
EUVE J0533+01.9	05 33 46	+01 57 29	202.0	−16.3	40	60	—	—	—	—	V371 Ori	GJ207.1	M3V	11.00	RE0533+015	—
EUVE J0536+23.4	05 36 53	+23 25 53	183.6	−4.6	—	—	—	—	23	—	HD245358	SAO77318	G0	8.9	—	A, G
EUVE J0536−47.9	05 36 58	−47 56 35	254.5	−31.9	50	—	—	—	—	—	HD37572	SAO217430	K0V	8.2	RE0536−475	—
EUVE J0545−59.9	05 45 16	−59 54 56	268.7	−31.4	20	—	—	—	—	—	SAO234124	CPD−59 509	G5	9.2	—	—
EUVE J0550−24.1	05 50 47	−24 07 55	229.1	−23.5	60	—	—	—	—	—	RE0550−240	—	DA1	16.7	RE0550−240	I1
EUVE J0552+15.8	05 52 27	+15 53 39	192.0	−5.3	1590	1220	—	—	3860*	—	WD0549+158	GD71	DA1	13.06	RE0552+155	B, I1
EUVE J0554+20.2	05 54 22	+20 16 52	188.5	−2.7	80	70	—	—	—	—	χ^1 Ori	HD39587	G0V	4.41	RE0554+201	—
EUVE J0558−37.5	05 58 11	−37 33 23	243.7	−26.1	30	80	—	—	—	—	RE0558−373	—	DA1	14.9	RE0558−373	I1
EUVE J0600+02.7	06 00 05	+02 42 45	204.6	−10.1	50	—	—	—	—	—	G 99 −49	—	M4	11.33	—	—
EUVE J0604+23.2	06 04 09	+23 13 54	187.0	0.7	—	—	—	—	19	—	1 Gem	HD41116	G5III	4.15	—	A, G
EUVE J0604−48.4	06 04 49	−48 26 27	255.9	−27.4	50	—	—	—	—	—	HD41824	HR2162	G6V	6.57	RE0604−482	—
EUVE J0604−34.5	06 04 51	−34 33 11	240.9	−24.0	20	—	—	—	—	—	RE0604−343	—	MVe	13.4	RE0604−343	—
EUVE J0605−48.3	06 05 04	−48 19 52	255.8	−27.4	30	—	—	—	—	—	RE0605−482	—	DA	16.0	RE0605−482	I1
EUVE J0612−16.7	06 12 44	−16 46 31	223.9	−16.0	30	—	—	—	—	—	SAO151224	BD−16 1396	K0	9.14	RE0612−164	—
EUVE J0616−64.9	06 16 54	−64 58 08	274.6	−28.0	4	—	—	—	—	—	RE0616−645	—	DA:	18.5	RE0616−645	—
EUVE J0618−72.0	06 18 29	−72 02 20	282.7	−28.2	15	—	—	—	—	—	HD45081	CPD−71 427	K3:V:	9.7	RE0618−720	—
EUVE J0622−17.9	06 22 43	−17 56 31	226.0	−14.3	—	—	560	4410	—	—	β CMa	HD44743	B1II/III	1.98	RE0622−175	D2
EUVE J0623−37.6	06 23 12	−37 40 41	245.4	−21.4	340	1930	70	—	—	—	RE0623−374	—	DA1	12.0	RE0623−374	I1
EUVE J0624−52.6	06 24 01	−52 41 21	261.2	−25.3	40	—	—	—	—	—	α Car	HD45348	F0II	−0.72	—	—
EUVE J0629−02.7	06 29 22	−02 47 46	212.9	−6.2	50	—	—	—	—	—	V577 Mon	GJ234A	M7Ve	11.1	RE0629−024	D3, E4
EUVE J0632−05.0	06 32 58	−05 05 22	215.4	−6.4	290	—	—	—	—	—	RE0632−050	—	DA1	15.6	RE0632−050	I1
EUVE J0633+10.7	06 33 50	+10 42 00	201.4	1.0	90	60	—	—	—	—	WD0631+107	KPD0631+1043	DA1	13.82	RE0633+104	I1
EUVE J0638−61.5	06 38 05	−61 31 56	271.2	−25.2	50	—	—	—	—	—	HD48189	HR2468	G1.5V	6.18	RE0637−613	—
EUVE J0640+09.8	06 40 56	+09 53 55	202.9	2.2	60	30	—	—	—	—	NOID	—	—	—	—	—
EUVE J0645−16.7	06 45 10	−16 42 09	227.2	−8.9	6590	1860	—	—	—	—	WD0642−166	Sirius B	DA2	8.44	RE0645−164	B
EUVE J0648−25.3	06 48 57	−25 23 16	235.6	−11.8	220	110	—	—	—	—	RE0648−252	—	DA1	13.8	RE0648−252	I1
EUVE J0651+22.8	06 51 23	+22 48 07	192.4	10.2	—	—	—	—	27	—	NOID	—	—	—	—	A, G
EUVE J0654−02.1	06 54 14	−02 08 40	215.2	−0.4	200	110	—	—	—	—	WD0651−020	GD80	DA1	14.2	RE0654−020	I1
EUVE J0658−28.9	06 58 40	−28 57 49	239.8	−11.3	—	80	4030	41840	—	—	ϵ CMa	HD52089	B2Iab:	1.50	RE0658−285	B, E6
EUVE J0702+12.9	07 02 03	+12 58 57	202.5	8.2	120	—	—	—	—	—	RE0702+125	—	Ke...	9.9	RE0702+125	—
EUVE J0710+38.5	07 10 05	+38 31 59	179.0	19.9	30	—	—	—	—	—	QY Aur	GJ268	M4.5evar	11.47	—	D3, E4
EUVE J0715−70.4	07 15 10	−70 24 44	281.6	−23.5	1020	40	—	—	—	—	RE0715−702	—	DA1	14.0	RE0715−702	I1
EUVE J0719+21.9	07 19 57	+21 57 11	196.0	15.8	—	—	—	—	67	—	δ Gem A	HD56986	F0IV	3.53	—	A, G
EUVE J0720−52.2	07 20 25	−52 17 15	263.6	−17.0	20	—	—	—	—	—	HD57852	HR2813	F1IV−V	6.05	—	—
EUVE J0720−31.7	07 20 49	−31 46 48	244.5	−8.2	240	120	—	—	—	—	RE0720−314	—	DA	15.1	RE0720−314	I1
EUVE J0723−27.7	07 23 21	−27 47 10	241.2	−5.9	640	460	—	—	—	—	RE0723−274	—	DA1	14.8	RE0723−274	I1
EUVE J0725−00.4	07 25 13	−00 24 29	217.2	7.3	30	—	—	—	—	—	BD−00 1712	AG−00 1021	K5	8.9	RE0725−002	—
EUVE J0729−38.7	07 29 09	−38 47 52	251.6	−9.9	100	—	—	—	—	—	HD59635	γ Pup	B5Vp	5.41	RE0729−384	H
EUVE J0734+31.8	07 34 36	+31 52 42	187.5	22.5	130	70	—	—	—	—	YY Gem	HD60179C	M1Ve	9.07	RE0734+315	—
EUVE J0739+05.2	07 39 18	+05 13 41	213.7	13.0	270	300	—	—	770*	—	α CMi	HD61421	F5IV	0.34	RE0739+051	B
EUVE J0743+28.8	07 43 17	+28 53 10	191.2	23.3	340	—	—	—	—	—	σ Gem	HD62044	K1III	4.28	RE0743+285	—
EUVE J0743−39.1	07 43 50	−39 10 48	253.3	−7.6	70	30	—	—	—	—	RE0743−391	—	DA	—	RE0743−391	I1
EUVE J0744+03.5	07 44 40	+03 33 23	215.9	13.5	60	—	—	—	—	—	YZ CMi	GJ285	M4.5V:e	11.12	RE0744+033	D3, E4
EUVE J0749−76.6	07 49 03	−76 41 32	288.9	−23.1	50	—	—	—	—	—	NOID	—	—	—	—	—
EUVE J0751+14.7	07 51 14	+14 43 46	206.1	19.8	40	—	—	—	—	—	RE0751+144	—	CV	14.5	RE0751+144	—
EUVE J0809−72.9	08 09 19	−72 59 01	285.8	−20.4	70	—	—	—	—	—	RE0809−725	—	DA	15.1	RE0809−725	I1
EUVE J0815−49.2	08 15 24	−49 13 28	264.9	−7.9	30	30	—	—	—	—	IX Vel	SAO219684	CVNL	9.44	RE0815−491	—
EUVE J0823−25.4	08 23 36	−25 24 59	246.1	6.8	70	—	—	—	—	—	HD70907	SAO175730	F3IV/V	8.8	RE0823−252	—
EUVE J0825−34.3	08 25 20	−34 21 55	253.7	2.0	20	—	—	—	—	—	HD71285	SAO199201	G1V	7.9	RE0825−342	—
EUVE J0831−53.6	08 31 56	−53 40 08	270.1	−8.2	50	—	—	—	—	—	RE0831−534	—	DA1	14.5	RE0831−534	I1
EUVE J0841+03.3	08 41 04	+03 21 30	223.0	25.8	320	60	—	—	—	—	RE0841+032	—	DA1	15.2	RE0841+032	I1
EUVE J0843−38.8	08 43 20	−38 52 16	259.5	2.2	30	—	—	—	—	—	HD74576	SAO199544	K1V	6.56	—	—
EUVE J0845+48.8	08 45 51	+48 52 35	170.6	38.6	280	180	—	—	—	—	HD74389B	BD+49 1766B	DA	15.5	RE0845+485	I1
EUVE J0846+06.4	08 46 47	+06 25 15	220.7	28.5	70	—	—	—	—	—	ϵ Hya	HD74874	G5III	3.38	RE0846+062	—
EUVE J0853−07.7	08 53 11	−07 42 58	235.1	22.7	30	—	—	—	—	—	HD75997	SAO136367	G5	9.2	RE0853−074	—
EUVE J0858+08.4	08 58 55	+08 28 59	220.2	32.1	30	—	—	—	—	—	G41−14	LHS6158	K:	10.89	RE0858+082	—
EUVE J0859−27.8	08 59 44	−27 48 54	253.0	11.8	70	—	—	—	—	—	TY Pyx	HD77137	G5V	6.90	RE0859−274	—
EUVE J0902−04.1	09 02 17	−04 06 14	233.2	26.6	40	—	—	—	—	—	RE0902−040	—	DA	12.4	RE0902−040	I1
EUVE J0908−37.1	09 08 20	−37 06 45	261.3	7.1	40	—	—	—	—	—	HD78644	SAO200016	G3V	8.3	RE0908−370	—
EUVE J0914+02.3	09 14 22	+02 19 10	228.8	32.5	110	40	—	—	—	—	θ Hya	HD79469	B9.5V	3.88	RE0914+021	—
EUVE J0916−19.7	09 16 57	−19 45 57	249.2	20.0	110	—	—	—	—	—	RE0916−194	—	DA:	17.3	RE0916−194	—
EUVE J0922+40.2	09 22 26	+40 12 02	182.0	45.3	90	50	—	—	—	—	BF Lyn	HD80715	K2V	7.63	RE0922+401	—
EUVE J0922+71.1	09 22 29	+71 10 08	141.7	37.4	—	—	15	—	—	—	NOID	—	—	—	RE0922+710	—
EUVE J0924−23.8	09 24 51	−23 48 33	253.7	18.7	40	—	—	—	—	—	IL Hya	HD81410	K2IV/Vp	7.90	RE0924−235	—
EUVE J0930+10.5	09 30 37	+10 35 26	222.2	40.1	30	—	—	—	—	—	HD82159	SAO98615	G5	7.6	RE0930+103	—
EUVE J0932−11.1	09 32 24	−11 11 08	244.6	28.4	70	—	—	—	—	—	LQ Hya	HD82558	K0Ve	7.80	RE0932−111	—
EUVE J0932+26.9	09 32 41	+26 58 14	201.2	46.1	40	—	—	—	—	—	HD82443	SAO80897	K0	7.01	—	—
EUVE J0934+69.8	09 34 24	+69 49 25	142.6	38.9	50	—	—	—	—	—	DK UMa	HD82210	G4III−IV	4.60	RE0934+694	—
EUVE J0940+50.3	09 40 26	+50 20 10	166.9	47.1	50	—	—	—	—	—	WD0937+505	PG0937+506	DA1	16.06	RE0940+502	I1
EUVE J0957+85.4	09 57 51	+85 29 16	126.5	30.4	80	—	—	—	—	—	RE0957+852	—	DA1	15.65	RE0957+852	I1
EUVE J1000+24.5	10 00 01	+24 32 38	206.9	51.5	50	40	—	—	—	—	DH Leo	HD86590	K0V...	8.45	RE1000+243	—
EUVE J1016−05.3	10 16 29	−05 20 37	248.0	40.4	650	—	—	—	—	—	RE1016−052	—	DA+M	14.3	RE1016−052	I1
EUVE J1019+19.8	10 19 36	+19 52 07	216.5	54.6	100	—	—	—	—	—	AD Leo	SAO81292	M4.5Ve	9.43	RE1019+195	—
EUVE J1019−14.1	10 19 52	−14 07 11	256.5	34.7	50	—	—	—	—	—	RE1019−140	—	DA1	15.4	RE1019−140	I1
EUVE J1024+26.3	10 24 08	+26 20 02	205.8	57.2	50	—	—	—	—	—	HD90052	SAO81330	G5	9.6	RE1024+262	—
EUVE J1027+32.3	10 27 08	+32 23 17	194.5	58.4	40	—	—	—	—	—	RE1027+322	—	—	—	RE1027+322	—
EUVE J1029+45.1	10 29 46	+45 07 12	170.9	56.6	60	40	—	—	—	—	WD1026+453	PG1026+454	DA1	16.09	RE1029+450	I1
EUVE J1032+53.4	10 32 10	+53 29 11	157.5	53.2	2160	850	—	—	—	—	RE1032+532	—	DA1	14.5	RE1032+532	I1
EUVE J1033−11.7	10 33 41	−11 42 17	257.7	38.8	80	—	—	—	—	—	WD1031−114	G 162−66	DA2	13.00	RE1033−114	I1
EUVE J1036+46.1	10 36 25	+46 07 59	168.4	57.3	120	90	—	—	—	—	WD1033+464	GD123	DA1+K	13.15	RE1036+460	I1
EUVE J1043+49.0	10 43 10	+49 02 11	162.7	57.0	370	100	—	—	—	—	RE1043+490	—	DA:	16.1	RE1043+490	B, I1

© American Astronomical Society • Provided by the NASA Astrophysics Data System

1994AJ....107..751M

TABLE 2. (continued)

EUVE Name	R.A. (J2000)	Decl. (J2000)	l	b	Lex c/ks	AlC c/ks	Dag c/ks	Tin c/ks	DSL c/ks	DSA c/ks	Possible ID	Other Name	Source Type	Mag	WFC Name	Notes
(1)	(2)	(3)	(4)	(5)	(6)	(7)	(8)	(9)	(10)	(11)	(12)	(13)	(14)	(15)	(16)	(17)
EUVE J1043+44.8	10 43 33	+44 53 04	169.6	58.9	30	—	—	—	—	—	PG1040+451	—	DA	16.94	RE1043+445	—
EUVE J1044+57.7	10 44 45	+57 44 18	150.1	52.2	70	—	—	—	—	—	WD1041+580	PG1041+580	DA1	14.59	RE1044+574	I1
EUVE J1046−49.4	10 46 48	−49 25 18	283.0	8.6	80	—	—	—	—	—	μ Vel	HD93497	G5III+...	2.69	RE1046−492	—
EUVE J1047−44.2	10 47 09	−44 16 06	280.6	13.2	—	—	70	—	—	—	NOID	—	—	—	—	—
EUVE J1051+54.0	10 51 36	+54 04 25	153.9	55.3	50	—	—	—	—	—	EK UMa	1E1048.5+5421	CVAM	18.0	RE1051+540	—
EUVE J1056+07.0	10 56 31	+07 01 20	244.1	56.1	20	—	—	—	—	—	CN Leo	GJ406	M6V:e	13.54	RE1056+070	—
EUVE J1058−38.7	10 58 21	−38 44 32	279.9	19.0	80	30	—	—	—	—	RE1058−384	—	DA	14.1	RE1058−384	I1
EUVE J1059+51.4	10 59 17	+51 24 17	156.3	57.8	980	110	—	—	—	—	LB1919	—	WD	16.8	RE1059+512	—
EUVE J1100+71.6	11 00 47	+71 37 22	134.5	42.9	290	70	—	—	—	—	WD1057+719	PG1057+719	DA1	14.95	RE1100+713	I1
EUVE J1104+38.2	11 04 27	+38 12 32	179.8	65.0	60	—	—	—	—	—	MKN421	—	BL Lac	12.69	RE1104+381	D1
EUVE J1104+45.0	11 04 28	+45 04 16	165.8	62.1	150	—	—	—	—	—	AN UMa	PG1101+453	CVAM	15.50	RE1104+450	—
EUVE J1111−22.8	11 11 40	−22 49 30	274.8	34.5	280	90	—	—	—	—	β Crt	HD97277	A1V+DA	4.48	RE1111−224	—
EUVE J1112+24.1	11 12 39	+24 09 15	215.0	67.6	150	—	—	—	—	—	WD1109+244	PG1109+244	DA1	15.93	RE1112+240	I1
EUVE J1118+31.5	11 18 11	+31 31 24	195.1	69.2	150	—	—	—	—	—	ξ UMa	HD98230J	G0V	3.78	RE1118+313	—
EUVE J1119+21.3	11 19 08	+21 19 38	223.3	68.2	30	—	—	—	—	—	PG1116+215	—	QSO	15.17	—	D1
EUVE J1126+18.6	11 26 18	+18 39 22	231.8	68.7	320	250	—	—	—	—	WD1123+189	PG1123+189	DAZ1	13.11	RE1126+183	I1
EUVE J1131−41.0	11 31 48	−41 02 40	287.1	19.4	50	—	—	—	—	—	GJ431	LHS2423	M3.5e	12.9	—	—
EUVE J1147+44.3	11 47 34	+44 18 59	155.5	68.6	30	—	—	—	—	—	PG1145+446	—	MV:e	15.44	RE1147+441	—
EUVE J1149−34.4	11 49 50	−34 24 12	288.7	26.8	—	—	70	—	—	—	NOID	—	—	—	—	—
EUVE J1149+28.7	11 49 51	+28 44 55	202.6	76.3	90	—	—	—	—	—	RE1149+284	—	CVAM	17.0	RE1149+284	—
EUVE J1201−03.7	12 01 45	−03 46 44	279.8	56.8	40	—	—	—	—	—	WD1159−034	PG1159−034	DQZO1	14.81	RE1201−034	—
EUVE J1203+44.5	12 03 11	+44 32 24	148.9	70.1	15	—	—	—	—	—	NGC4051	1H1205+440	AGN	10.14	—	D1
EUVE J1215+72.5	12 15 43	+72 32 14	126.7	44.3	30	—	—	—	—	—	DK Dra	HD106677	K0III	6.29	—	—
EUVE J1225+25.5	12 25 01	+25 33 55	226.2	83.9	30	—	—	—	—	—	IL Com	HD108102	F8	8.16	RE1225+253	—
EUVE J1229+02.0	12 29 08	+02 03 04	290.0	64.4	40	—	—	—	—	—	3C 273	1H1226+023	QSO	12.86	—	D1
EUVE J1235+23.5	12 35 20	+23 34 13	256.4	84.9	20	—	—	—	—	—	WD1232+238	PG1232+238	DA1	15.66	RE1235+233	I1
EUVE J1236+47.9	12 36 45	+47 55 05	129.8	69.0	940	430	—	—	—	—	WD1234+482	PG1234+482	DAZ1	14.38	RE1236+475	I1
EUVE J1241−01.4	12 41 39	−01 26 29	297.8	61.3	70	60	—	—	—	—	γ Vir	HD110379	F0V	3.65	—	—
EUVE J1251+27.5	12 51 42	+27 31 53	114.7	89.6	30	—	—	—	—	—	31 Com	HD111812	G0IIIp	4.94	RE1251+273	—
EUVE J1255+25.8	12 55 32	+25 52 51	339.5	88.5	30	—	—	—	—	—	IN Com	HD112313	G5III	8.7	RE1255+255	—
EUVE J1257+22.0	12 57 01	+22 01 24	317.2	84.7	3870	3140	220	290	—	—	WD1254+223	GD153	DA1	13.40	RE1257+220	B, I1
EUVE J1257+35.2	12 57 41	+35 12 40	113.9	81.8	30	—	—	—	—	—	BF CVn	—	M0V	10.5	RE1257+351	D3, E4
EUVE J1300+12.3	13 00 49	+12 21 39	311.9	75.1	40	—	—	—	—	—	DT Vir	BD+13 861	M1.5e	10.34	—	D3, E4
EUVE J1309+08.2	13 09 24	+08 14 15	316.4	70.6	—	—	40	—	—	—	RE1309+081	—	—	—	RE1309+081	—
EUVE J1316+29.0	13 16 21	+29 05 30	54.0	84.2	29370	19230	1330	1370	—	—	HZ 43	WD1314+293	DA1	12.9	RE1316+290	B, I1
EUVE J1316+09.4	13 16 45	+09 25 13	322.8	71.3	40	30	—	—	—	—	59 Vir	HD115383	G0Vs	5.22	RE1316+092	—
EUVE J1332+22.4	13 32 43	+22 29 53	8.9	79.6	30	—	—	—	—	—	BD+23 2581	—	star	9.67	RE1332+223	—
EUVE J1334+37.1	13 34 46	+37 09 56	83.3	76.4	160	—	—	—	—	—	BH CVn	HD118216	F2IV	4.98	RE1334+371	—
EUVE J1352+69.2	13 52 56	+69 17 58	115.1	46.9	40	—	—	—	—	—	MKN279	1H1350+696	AGN	14.57	—	D1
EUVE J1409−45.2	14 09 05	−45 17 57	317.0	15.4	280	—	—	—	—	—	V834 Cen	H1405−45	CVAM	14.2	—	—
EUVE J1425+51.8	14 25 09	+51 50 15	93.8	59.7	50	—	—	—	—	—	θ Boo	HD126660	F7V	4.10	RE1425+515	—
EUVE J1426+50.0	14 26 42	+50 05 30	91.0	60.7	50	—	—	—	—	—	RE1426+500	—	DA2+MVe	14.0	RE1426+500	—
EUVE J1428+42.6	14 28 33	+42 40 31	77.5	64.9	30	—	—	—	—	—	1H1430+423	H1426+428	BL Lac	—	RE1428+424	D1
EUVE J1430−62.6	14 30 23	−62 38 27	314.0	−1.9	30*	30*	—	—	—	—	Prox. Cen	V645 Cen	M5Ve	11.05	RE1429−624	E4
EUVE J1434−60.4	14 34 18	−60 25 50	315.3	−0.1	20	—	—	—	—	—	V841 Cen	HD127535	K1IV/Ve	8.49	RE1434−602	—
EUVE J1438+64.2	14 38 57	+64 17 18	105.5	49.0	40	—	—	—	—	—	HD129333	SAO16453	G0Ve	7.54	RE1438+641	—
EUVE J1439−60.8	14 39 42	−60 51 28	315.7	−0.7	440	490	8	12	—	—	α Cen	HD128620J	G0	−0.1	RE1439−605	B, E4
EUVE J1439+75.0	14 39 54	+75 05 10	114.1	40.1	110	—	—	—	—	—	RE1440+750	—	DA1	15.1	RE1440+750	I1
EUVE J1445+63.4	14 45 58	+63 29 01	103.8	49.2	50	—	—	—	—	—	RE1446+632	—	DA1	16.1	RE1446+632	I1
EUVE J1451+19.1	14 51 24	+19 06 46	23.1	61.4	130	50	—	—	—	—	ξ Boo	HD131156	G8V	4.55	RE1451+190	—
EUVE J1501−43.6	15 01 17	−43 39 50	326.4	13.2	40	—	—	—	—	—	RE1501−433	—	MVe	11.9	RE1501−433	—
EUVE J1502+66.1	15 02 04	+66 11 51	104.7	46.0	5900	30	—	—	—	—	WD1501+664	H1504+65	DZQ1	—	RE1502+661	—
EUVE J1503+47.6	15 03 47	+47 38 28	80.3	57.1	150	40	—	—	—	—	44 Boo	—	G2+G0Vnvar	—	RE1503+473	—
EUVE J1507+76.1	15 07 49	+76 11 34	113.1	38.2	30	—	—	—	—	—	HD135363	SAO8175	G5	9.2	—	—
EUVE J1511+61.8	15 11 51	+61 51 25	98.9	48.2	30	—	—	—	—	—	BV Dra	HD135421	F7V	7.88	RE1511+615	—
EUVE J1521+52.3	15 21 43	+52 21 07	85.3	52.4	70	—	—	—	—	—	WD1520+525	PG1520+525	DQOZ1	16.6	RE1521+522	—
EUVE J1521+20.9	15 21 53	+20 58 02	31.0	55.2	60	—	—	—	—	—	BPM90688	—	M0Ve	10.1	RE1521+205	—
EUVE J1529+80.4	15 29 22	+80 26 33	115.6	34.3	30	—	—	—	—	—	HD139813	SAO2558	G5	7.31	RE1529+802	—
EUVE J1535−77.4	15 35 41	−77 24 56	311.6	−17.4	60	—	—	—	—	—	NOID	—	—	—	—	—
EUVE J1538−57.7	15 38 58	−57 42 44	323.8	−1.8	30	—	—	—	—	—	V343 Nor	HD139084	K0V	8.1	RE1538−574	—
EUVE J1545−30.3	15 45 50	−30 22 03	341.9	19.0	50	—	—	—	—	—	HD140637	SAO206946	K2V	9.4	RE1545−302	—
EUVE J1546−36.7	15 46 59	−36 46 43	337.8	13.9	70	—	—	—	—	—	RE1546−364	—	DA	15.7	RE1546−364	I1, I2
EUVE J1601+51.3	16 01 50	+51 22 45	80.5	47.0	40	—	—	—	—	—	HD144110	SAO29761	G5	8.5	RE1601+512	—
EUVE J1603−57.7	16 03 33	−57 46 58	326.3	−3.9	50	—	—	—	—	—	ι^1 Nor	HD143474	A7IV	4.63	RE1603−574	—
EUVE J1604−21.9	16 04 02	−21 55 38	351.3	22.4	30	—	—	—	—	—	HD143937	SAO184077	K0V	8.65	—	—
EUVE J1614+33.8	16 14 40	+33 51 26	54.7	46.1	430	80	—	—	—	—	σ CrB	HD146361J	G0	5.64	RE1614+335	—
EUVE J1617+55.2	16 17 09	+55 17 49	84.9	43.7	40	—	—	—	—	—	CR Dra	GJ616.2	M1Ve	9.96	RE1617+551	—
EUVE J1619−15.6	16 19 57	−15 39 33	359.1	23.8	270	—	—	—	—	—	Sco X−1	1H1617−155	LMXB	—	RE1619−153	—
EUVE J1623−39.2	16 23 31	−39 13 44	341.5	7.3	310	90	—	—	960*	300*	WD1620−391	CD−38 10980	DA2	11.0	RE1623−391	B, E8, I1
EUVE J1623−39.2b	16 23 34	−39 14 11	341.5	7.2	—	—	—	—	60*	100*	HD147513	HR6094	G5V	5.40	—	C, E4
EUVE J1625−49.1	16 25 10	−49 09 37	334.6	0.1	40	—	—	—	—	—	HD147633	SAO226738	K0/K1V:+...	7.1	RE1625−490	—
EUVE J1629+78.0	16 29 02	+78 04 48	111.3	33.6	1540	100	—	—	—	—	RE1629+780	—	DA1	13.28	RE1629+780	I1
EUVE J1636+52.8	16 36 10	+52 53 43	80.9	41.5	30	—	—	—	—	—	HD150100	16 Dra	B9.5Vn	5.53	RE1636+525	H
EUVE J1638+34.9	16 38 24	+34 58 19	56.9	41.4	80	—	—	—	—	—	WD1636+351	PG1636+351	DA1	14.18	RE1638+350	I1
EUVE J1650+40.6	16 50 20	+40 36 39	64.6	39.6	20	—	—	—	—	—	RE1650+403	—	DA1	14.5	RE1650+403	I1
EUVE J1653+39.7	16 53 52	+39 45 07	63.6	38.9	30	—	—	—	—	—	MKN501	1H1651+398	BL Lac	12.96	—	D1
EUVE J1655−08.3	16 55 29	−08 20 27	11.0	21.1	120	40	—	—	—	—	Wolf630	HD152751	M3Ve	9.04	RE1655−081	—
EUVE J1656+65.1	16 56 03	+65 08 10	95.7	36.5	15	—	—	—	—	—	19 Dra	HD153597	F6Vvar	4.89	RE1656+650	—
EUVE J1656−39.1	16 56 43	−39 07 38	345.9	2.5	120	—	—	—	—	—	HD152705	SAO208217	K3/K4V	8.5	RE1656−390	—
EUVE J1657+35.3	16 57 49	+35 20 21	58.1	37.5	160	—	—	—	—	—	Her X−1	HZ Her	XRB puls	—	RE1657+352	B
EUVE J1659+44.0	16 59 47	+44 01 01	69.1	38.1	160	90	—	—	—	—	WD1658+441	PG1658+44	DA1p	14.87	RE1659+440	I1
EUVE J1711+66.7	17 11 18	+66 44 42	97.2	34.6	10	—	—	—	—	—	RE1711+664	—	DA1	17.1	RE1711+664	—
EUVE J1717−66.9	17 17 28	−66 56 52	324.9	−16.3	100	—	—	—	—	—	V824 Ara	HD155555	G5IV	6.67	RE1717−665	—
EUVE J1726+58.6	17 26 41	+58 37 47	87.2	33.8	50	—	—	—	—	—	WD1725+586	LB 335	DA1	15.45	RE1726+583	I1
EUVE J1727−35.9	17 27 41	−35 59 46	352.0	−0.6	70	—	—	—	—	—	RE1727−355	—	DA	—	RE1727−355	I2
EUVE J1732+74.2	17 32 38	+74 14 00	105.5	31.4	30	—	—	—	—	—	DR Dra	HD160538	K0III	6.55	RE1732+741	—
EUVE J1734+61.8	17 34 57	+61 53 10	91.0	32.7	15	—	—	—	—	—	26 Dra	HD160269	G0Va	5.23	—	—
EUVE J1736+68.7	17 36 47	+68 45 36	99.1	31.9	20	15	—	—	—	—	ω Dra	HD160922	F5V	4.80	RE1736+684	—
EUVE J1738+61.2	17 38 37	+61 14 48	90.2	32.2	15	—	—	—	—	—	AC+61 27026	—	K8V	10.3	RE1738+611	—
EUVE J1746−70.6	17 46 14	−70 39 51	322.7	−20.3	250	40	—	—	—	—	RE1746−703	—	DA	16.5	RE1746−703	I1

© American Astronomical Society • Provided by the NASA Astrophysics Data System

1994AJ....107..751M

TABLE 2. (continued)

EUVE Name	R.A. (J2000)	Decl. (J2000)	l	b	Lex c/ks	AIC c/ks	Dag c/ks	Tin c/ks	DSL c/ks	DSA c/ks	Possible ID	Other Name	Source Type	Mag	WFC Name	Notes
(1)	(2)	(3)	(4)	(5)	(6)	(7)	(8)	(9)	(10)	(11)	(12)	(13)	(14)	(15)	(16)	(17)
EUVE J1755+36.1	17 55 22	+36 11 26	62.1	26.3	40	—	—	—	—	—	HD163621	SAO66472	G5	7.9	RE1755+361	—
EUVE J1757+29.2	17 57 44	+29 14 26	54.9	23.8	30	—	—	—	—	—	ζ Her	HD163993	G8III	3.70	—	—
EUVE J1800+68.6	18 00 07	+68 36 45	98.7	29.8	70	—	—	—	—	—	KUV18004+6836	—	DA1	14.74	RE1800+683	I1
EUVE J1805+02.4	18 05 28	+02 29 55	29.9	11.4	70	90	—	—	—	—	70 Oph	HD165341	K0V	4.03	—	—
EUVE J1805+21.4	18 05 51	+21 26 20	47.8	19.3	70	—	—	—	—	—	V772 Her	HD165590	G0	7.07	RE1805+212	—
EUVE J1808+29.6	18 08 16	+29 41 24	56.2	21.8	70	—	—	—	—	—	V815 Her	HD166181	G5	7.66	RE1808+294	—
EUVE J1816+49.8	18 16 11	+49 52 08	77.9	25.9	2500	50	—	—	—	—	AM Her	H1816+49	CVAM	—	—	—
EUVE J1820+58.0	18 20 25	+58 04 53	87.0	26.8	140	—	—	—	—	—	RE1820+580	—	DA1	13.8	RE1820+580	—
EUVE J1821+64.3	18 21 44	+64 22 03	94.0	27.4	15	—	—	—	—	—	K1–16	WD1821+643	CSPN/DQOZ1	15.0	RE1821+642	—
EUVE J1833+51.7	18 33 51	+51 43 23	80.6	23.6	60	—	—	—	—	—	BY Dra	HD234677	K6Ve	8.07	RE1833+514	—
EUVE J1834+18.6	18 34 19	+18 41 11	47.9	12.1	50	—	—	—	—	—	HD171488	SAO103862	G0V	7.30	RE1834+184	—
EUVE J1836+38.7	18 36 54	+38 47 16	67.4	19.2	110	—	—	—	—	—	α Lyr	HD172167	A0V	0.03	—	—
EUVE J1845–74.3	18 45 00	−74 20 21	320.3	−25.6	80	—	—	—	—	—	RE1844–741	—	CV	17.6	RE1844–741	—
EUVE J1845+68.3	18 45 06	+68 22 26	98.8	25.7	50	—	—	—	—	—	KUV18453+6819	—	DA1	15.0	RE1845+682	E8
EUVE J1847+01.9	18 47 38	+01 57 34	34.2	1.7	490	220	—	—	1410*	1180*	WD1845+019	Lanning 18	DA1	12.96	RE1847+015	B, E8, I1
EUVE J1847–22.3	18 47 57	−22 20 15	12.5	−9.3	80	—	—	—	—	—	RE1847–221	—	DA1	13.9	RE1847–221	I1
EUVE J1849–23.8	18 49 49	−23 50 31	11.3	−10.3	60	—	—	—	—	—	V1216 Sgr	GJ729	M4.5V:e	10.95	—	—
EUVE J1855+23.5	18 55 53	+23 33 42	54.6	9.6	70	—	—	—	—	—	V775 Her	HD175742	K0	8.09	RE1855+233	—
EUVE J1907+30.2	19 07 31	+30 15 33	61.9	10.1	90	—	—	—	—	—	V478 Lyr	—	G8V	—	RE1907+301	—
EUVE J1914+19.3	19 14 39	+19 19 29	52.7	3.8	45	—	—	—	—	—	Ross 733	G185–12	M:	13.0	—	—
EUVE J1918+59.9	19 18 24	+59 59 50	91.0	20.0	30	—	—	—	—	—	LB342	—	star	14.3	RE1918+595	—
EUVE J1925–56.5	19 25 59	−56 34 08	340.6	−27.0	700	—	—	—	—	—	RE1925–563	—	—	—	RE1925–563	—
EUVE J1938–46.2	19 38 35	−46 13 18	352.4	−27.1	120	—	—	—	40*	—	RE1938–461	—	CVAM	15.2	RE1938–461	B, E7
EUVE J1943+50.0	19 43 38	+50 04 40	83.1	12.8	30	—	—	—	—	—	RE1943+500	—	DA1	14.4	RE1943+500	I1
EUVE J1959+22.7	19 59 35	+22 43 11	60.8	−3.7	40	—	—	—	—	—	NGC6853	Dumbell Neb.	CSPN	7.5	RE1959+224	—
EUVE J2000–33.7	20 00 22	−33 42 13	7.3	−28.2	60	—	—	—	—	—	HD189245	HR7631	F7V	5.66	RE2000–334	—
EUVE J2004–56.0	20 04 18	−56 03 15	341.8	−32.3	40	—	—	—	—	—	WD2000–562	—	DA	15.2	RE2004–560	I1
EUVE J2005+22.6	20 05 41	+22 39 56	61.5	−4.9	240	—	—	—	—	—	QQ Vul	—	CVAM	14.4	RE2005+224	—
EUVE J2009–60.4	20 09 05	−60 25 59	336.6	−32.9	2270	400	—	—	—	—	RE2009–602	—	DA:	13.4	RE2009–602	—
EUVE J2013+40.0	20 13 09	+40 02 36	77.0	3.2	100	—	—	—	—	—	RE2013+400	—	DA1	13.8	RE2013+400	I1
EUVE J2018–57.3	20 18 50	−57 22 05	340.2	−34.2	40	—	—	—	—	—	WD2014–575	L210–114	DA2	13.8	RE2018–572	I1
EUVE J2024–42.4	20 24 01	−42 25 01	358.3	−34.5	130	—	—	—	300*	130*	MCT2020–4234	—	DA	14.7	RE2023–422	B, I1
EUVE J2024+20.0	20 24 14	+20 00 19	61.7	−10.0	40	—	—	—	—	—	RE2024+200	—	DA1	16.4	RE2024+200	—
EUVE J2030+52.6	20 30 28	+52 37 50	89.1	7.8	110	90	—	—	—	—	V1974 Cyg	Nova Cyg 1992	Nova	—	—	E9, D4
EUVE J2037+75.5	20 37 05	+75 35 58	109.2	20.1	60	—	—	—	—	—	VW Cep	HD197433	K0Vvar	7.38	RE2037+753	—
EUVE J2041–32.4	20 41 49	−32 25 39	11.1	−36.3	—	—	—	—	800*	140*	AT Mic	HD196982	M4Ve	10.25	RE2041–322	B, J
EUVE J2045–31.3	20 45 06	−31 21 10	12.6	−36.8	250	—	—	—	5250*	150*	AU Mic	HD197481	M0Ve	8.61	RE2045–312	B, E5, J
EUVE J2053–17.5	20 53 35	−17 34 45	29.6	−34.7	—	—	—	—	20	—	NOID	—	—	—	—	A, G
EUVE J2055–17.1	20 55 49	−17 07 05	30.4	−35.0	70	—	—	—	246	—	HD199143	SAO163989	F8V	7.1	RE2055–170	G
EUVE J2056–17.1	20 56 04	−17 10 16	30.3	−35.1	—	—	—	—	282	—	NOID	—	—	—	—	A, G
EUVE J2100+40.0	21 00 00	+40 04 36	82.4	−3.9	40	—	—	—	—	—	V1396 Cyg	GJ815A	M3Ve	10.1	RE2100+400	D3, E4
EUVE J2102+27.7	21 02 25	+27 47 37	73.3	−12.3	50	—	—	—	—	—	ER Vul	HD200391	G0V+...	7.27	RE2102+274	—
EUVE J2104–77.0	21 04 55	−77 01 48	315.9	−33.7	30	—	—	—	—	—	α Oct	HD199532	A7III+...	5.15	—	—
EUVE J2105–16.9	21 05 46	−16 54 16	31.7	−37.1	—	—	—	—	11	—	BD–17 6172	—	K7	9.7	—	A, G
EUVE J2108–05.2	21 08 01	−05 17 09	44.8	−32.6	40	—	—	—	—	—	RE2107–051	—	CV	15.3	RE2107–051	—
EUVE J2112+50.1	21 12 45	+50 06 35	91.4	1.1	460	220	—	—	—	—	WD2111+498	GD394	DA1	13.09	RE2112+500	B, I1
EUVE J2114+50.3	21 14 41	+50 18 12	91.7	1.0	20	—	—	—	—	—	NOID	—	—	—	—	—
EUVE J2116+73.8	21 16 53	+73 51 02	109.4	16.9	100	—	—	—	—	—	KUV21168+7338	—	DA1	15.11	RE2116+735	I1
EUVE J2121+40.3	21 21 00	+40 20 40	85.4	−6.7	30	—	—	—	—	—	HD203454	HR8170	F8V	6.40	RE2121+402	—
EUVE J2126+19.3	21 26 26	+19 22 23	70.4	−22.0	540	420	—	—	—	—	IK Peg	HD204188	A8m+DA	6.07	RE2126+192	I1
EUVE J2127–22.2	21 27 42	−22 12 12	27.3	−43.8	80	—	—	—	—	—	RE2127–221	—	DA1	14.7	RE2127–221	I1
EUVE J2131+23.3	21 31 03	+23 20 49	74.3	−20.1	40	—	—	—	—	—	BD+22 4409	G145–43	K8	9.25	—	—
EUVE J2141–14.0	21 41 34	−14 02 56	39.6	−44.0	40	—	—	—	109	—	HR8283	—	G2V	5.18	—	G
EUVE J2147–16.1	21 47 03	−16 07 51	37.6	−46.0	70	—	—	—	—	—	42 Cap	HD207098	A7IIIm	2.87	RE2147–160	—
EUVE J2154–30.4	21 54 55	−30 29 41	17.1	−51.4	80	—	—	—	—	—	MCT2151–3043	—	DA1	14.7	RE2154–302	I1
EUVE J2156–54.6	21 56 22	−54 38 44	339.7	−48.1	2060	780	—	—	—	—	RE2156–543	—	DA1	14.5	RE2156–543	I1
EUVE J2156–41.7	21 56 34	−41 42 23	359.1	−51.6	190	—	—	—	—	—	MCT2153–4156	—	DA	15.5	RE2156–414	I1
EUVE J2158+82.8	21 58 34	+82 52 54	117.7	21.8	140	—	—	—	—	—	HD209943	SAO3675	F5	7.49	RE2158+825	—
EUVE J2158–30.2	21 58 52	−30 13 55	17.7	−52.2	250	—	—	—	570*	—	PKS2155–304	1H2156–304	BL Lac	14.0	RE2158–301	B, D1, E2
EUVE J2207+25.3	22 07 47	+25 19 57	82.4	−24.4	30	—	—	—	—	—	RE2207+252	—	DA1	14.4	RE2207+252	I1
EUVE J2208+45.7	22 08 40	+45 44 49	95.6	−8.3	100	7**	—	—	—	—	AR Lac	HD210334	G2IV+K0IV	6.11	RE2208+454	B, E3
EUVE J2209–47.1	22 09 15	−47 09 37	349.6	−52.6	30	—	—	—	—	—	NGC7213	PKS2206–474	AGN	10.27	—	D1
EUVE J2210–30.0	22 10 31	−30 05 46	18.4	−54.7	110	—	—	—	—	—	RE2210–300	—	DA1	14.2	RE2210–300	I1
EUVE J2213–11.1	22 13 12	−11 10 26	48.4	−49.6	—	—	—	—	44	—	HD210803	—	G5	9.31	—	A, G
EUVE J2214–49.3	22 14 15	−49 19 33	345.8	−52.6	1010	4790	120	—	—	—	RE2214–491	—	DA1	11.5	RE2214–491	I1
EUVE J2220+49.5	22 20 05	+49 30 38	99.3	−6.3	50	—	—	—	—	—	BD+48 3686	SAO51891	K0	8.1	RE2220+493	—
EUVE J2226–16.7	22 26 36	−16 44 45	42.6	−55.0	50	—	—	—	—	—	53 Aqr	HD212698	G3V	6.35	—	—
EUVE J2228+57.6	22 28 07	+57 41 25	104.7	−0.0	30	—	—	—	—	—	DO Cep	HD239960B	M4.5V:e	10.30	—	—
EUVE J2238–20.6	22 38 46	−20 36 59	37.8	−59.1	150	50	—	—	—	—	FK Aqr	HD214479	M0Vpe	9.07	RE2238–203	—
EUVE J2244–32.3	22 44 46	−32 20 18	14.5	−62.1	30	—	—	—	—	—	PHL396	TON S 72	DA	15.8	RE2244–321	I1
EUVE J2246+44.3	22 46 48	+44 20 14	100.6	−13.1	90	—	—	—	—	—	EV Lac	GJ873	M4.5V:e	10.09	RE2246+442	—
EUVE J2249+58.5	22 49 56	+58 35 03	107.6	−0.6	120	—	—	—	—	—	LAN 23	—	star	14.	RE2249+583	—
EUVE J2300–07.0	23 00 37	−07 04 16	65.2	−56.9	70	—	—	—	375	—	BD–07 5906	HD217411	G5	9.8	RE2300–070	G
EUVE J2301–39.2	23 01 14	−39 17 34	357.9	−64.1	—	—	90	—	—	—	NOID	—	—	—	—	—
EUVE J2309+47.9	23 09 56	+47 57 30	105.9	−11.5	50	30	—	—	—	—	KZ And	HD218738	G5	7.91	RE2309+475	—
EUVE J2312+10.7	23 12 19	+10 46 37	87.2	−45.1	2040	790	—	—	8420*	—	WD2309+105	GD246	DAZ1	13.11	RE2312+104	B, E1, I1
EUVE J2319+79.0	23 19 25	+79 00 38	118.5	16.9	110	30	—	—	—	—	V368 Cep	HD220140	G9V	7.54	RE2319+790	—
EUVE J2321–26.9	23 21 17	−26 59 44	28.1	−70.0	40	—	—	—	—	—	HD220096	HR8883	G4V	5.64	—	—
EUVE J2324–54.7	23 24 31	−54 42 00	326.9	−58.2	480	180	—	—	—	—	RE2324–544	—	DA	15.3	RE2324–544	I1
EUVE J2329+41.4	23 29 28	+41 27 52	106.8	−18.8	40	—	—	—	—	—	G190–27	—	M2	12.42	—	—
EUVE J2331+19.9	23 31 53	+19 56 30	98.6	−39.1	110	—	—	—	—	—	EQ Peg	GJ896A	M4Ve:+...	10.32	RE2331+195	—
EUVE J2334–47.2	23 34 03	−47 14 41	334.8	−64.8	280	620	—	—	—	—	MCT2331–4731	—	DA1	13.3	RE2334–471	I1
EUVE J2337+46.4	23 37 31	+46 27 51	109.9	−14.5	270	—	—	—	—	—	λ And	HD222107	G8III	3.82	RE2337+462	—
EUVE J2339–69.2	23 39 37	−69 12 11	312.1	−46.6	20	—	—	—	—	—	HD222259	SAO255538	G6:IV+...	8.0	RE2339–691	—
EUVE J2352+75.5	23 52 22	+75 32 28	119.2	13.1	30	—	—	—	—	—	HD223778	HR9038	K3V	6.39	RE2352+753	—
EUVE J2353–24.5	23 53 07	−24 32 12	40.9	−76.6	60	—	—	—	—	—	MCT2350–2448	—	DA1	15.1	RE2353–243	I1
EUVE J2353–70.3	23 53 10	−70 23 38	309.9	−45.9	410	880	—	—	—	—	HD223816	CPD–71 2778	F5IV+DA	8.8	RE2353–702	—
EUVE J2355+28.6	23 55 01	+28 37 52	108.2	−32.6	150	30**	—	—	—	—	II Peg	HD224085	K0V...	7.37	RE2355+283	B, E3

© American Astronomical Society • Provided by the NASA Astrophysics Data System

1994AJ....107..751M

Notes to TABLE 2

†Table 2 is presented in its complete form in the ApJ/AJ CD-ROM Series, Volume 2, 1994.
*Count rate derived from the calibration observation.
**Count rate from Patterer *et al.* (1993).
A Source verified using only the skymaps.
B Calibration target.
C Serendipitous source observed during a calibration pointing.
D# Private communication from: 1. H. Marshall, T. Carone, & A. Fruscione; 2. J. Vallerga; 3. P. Vedder; 4. G. Stringfellow.
E# Refer to the following papers: 1. Vennes *et al.* (1993); 2. Marshall, Carone, & Fruscione (1993); 3. Patterer *et al.* (1993); 4. Vedder *et al.* (1993); 5. Cully *et al.* (1993); 6. Vallerga, Vedder, & Welsh (1993); 7. Warren *et al.* (1993); 8. Finley *et al.* (1993); 9. Stringfellow & Bowyer (1993).
F Three stars, including a white dwarf, are very likely optical counterparts (J. Dupuis, private communication).
G DS count rates, accurate to 50%, are provided by J. Vallerga.
H A and B stars probably detected as a "UV leak" by *EUVE* but reported as extreme ultraviolet sources in the *ROSAT Bright Source Catalog.*
I# Optical ID confirmed via: 1. High signal-to-noise optical spectra by D. Finley; 2. Photometry or spectroscopy by M. Dopita.
J The DS count rate includes the flare occurring during the observation.

x-ray binary. Table 4 is a breakdown of the BSL sources by spectral type.

Column 15. The visual magnitude of the optical counterparts. The measurements generally come from the variety of catalogues included in SIMBAD and NED databases and therefore should be considered only as a rough indication. See Fig. 5 for a plot of the visual magnitude of the optical counterpart versus the EUV count rate. We observe that 92% of white dwarf stars are fainter than $m_V \sim 13$ but are the brightest EUV sources, while 96% of late-type stars are brighter than $m_V \sim 11$ but lie within the lower two decades of EUV count rate.

Column 16. Where applicable, the name of the EUV source as it appears in the *ROSAT* WFC Bright Source Catalogue (Pounds *et al.* 1993). *EUVE* and *ROSAT* sources are considered identical if they lie within 1.5 arcmin of one another.

Column 17. General notes and/or comments about specific EUV sources (e.g., which sources were calibration targets); all notes are explained at the end of Table 2.

5. SURFACE DENSITY OF EUV SOURCES

Given the distribution of source intensities, we have computed the sky angular surface density of sources given an estimate of the sky coverage function. We have generated an approximation to the sky coverage function using the pigeonhole data for arbitrarily placed points on the sky, without producing a detailed map of the sky that gives the sensitivity limits appropriate for the detection runs used to find the sources.

TABLE 3. BSL sources by filter detection.

Scanners				Deep survey	
Lexan/B	Al/Ti/C	Dagwood	Tin	Lexan/B	Al/C
327	92	17	11	39	6

TABLE 4. BSL sources by classification.

Number	Classification
172	Late-type stars
117	White dwarfs
14	Cataclysmic variables
10	Extragalactic objects
6	A stars
7	B stars
15	Other
15	No ID
356	Total BSL Sources

5.1 Sky Coverage

In order to calculate the sky coverage included in the BSL, we added locations to the master pigeonhole catalogue at every 10° in right ascension and declination as well as one each at the celestial poles. There are 614 locations in this grid. Although the grid points are not equally spaced on the sky, they were chosen without regard to either the survey strategy (which places emphasis on the ecliptic pole and may have gaps along ecliptic longitude lines) or to the actual distribution of sources (the grid was determined long before the survey and before the preliminary results from the WFC survey were available).

The pigeonhole for each grid position was handled in exactly the same way as for those that were expected to contain sources, except that the "source" location was not allowed to vary. For detected sources with total count rate estimate R and uncertainty σ_R, an empirical relation between the SNR, defined as R/σ_R, and the square root of the significance, ΔS (see Sec. *3.3*), indicates that a source with a significance of 36 is expected to have a SNR of about four. For grid sources, then, the sensitivity was set to $4\sigma_R$, the uncertainty as derived by the flux measurement software. The declination of the grid position was used to

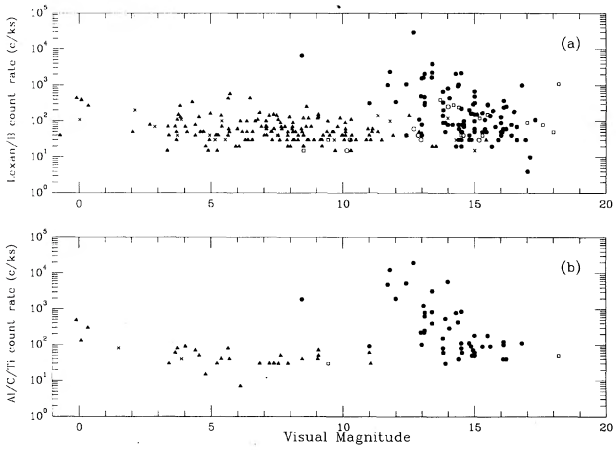

FIG. 5. Plot of the EUV count rate vs visual magnitude for the following classes of objects: white dwarf stars (filled circles), late-type stars (filled triangles), cataclysmic variables (empty squares), extragalactic objects (empty circles), and other objects (crosses).

© American Astronomical Society • Provided by the NASA Astrophysics Data System

1994AJ....107..751M

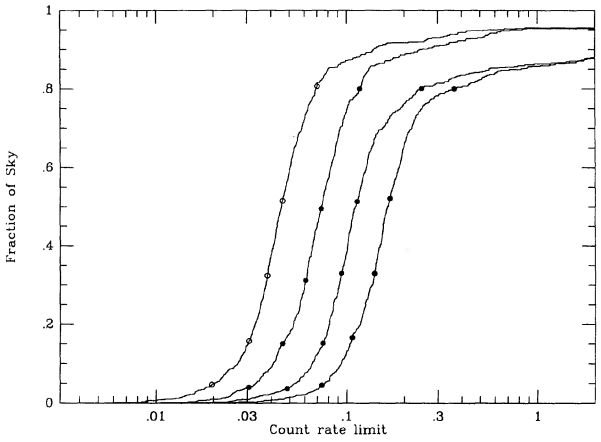

FIG. 6. Coverage functions for each *EUVE* bandpass, given as fraction of the sky surveyed as a function of count rate. Curve with open circles: Lexan/B band; solid stars: Al/Ti/C band; open stars: Dagwood; solid circles: tin band.

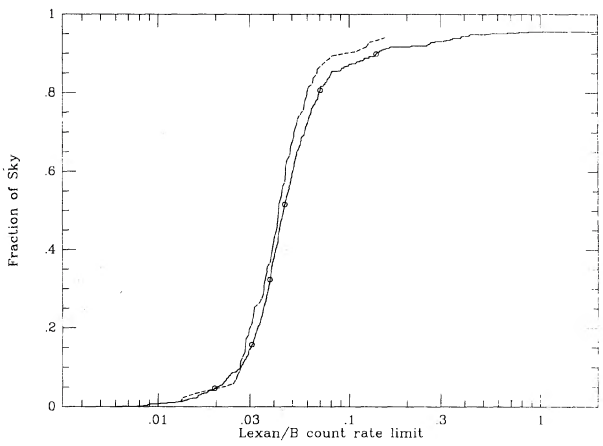

FIG. 8. Sky coverage functions for the Lexan/B band derived by two different methods. Solid curve with open circles: method using grid sources; thin dashed curve: method using source count rates from this paper. The two are reasonably close, so the grid source method may be used for each bandpass, even when there are very few detected sources.

estimate the size of the region for which this sensitivity was effective. The angular size of the region, in steradians, is given by

$$\omega(\delta)=\frac{4\pi}{2\times 36}[\sin(\delta+5^\circ)-\sin(\delta-5^\circ)] \quad (1)$$

and at the poles the angular size of the 5° radius region was used. For each location with coordinates (α_i,δ_i) there is a value of R_i and ω_i, so the sky coverage function may be formed

$$\Omega(R)=\sum_{R_i<R}\omega_i, \quad (2)$$

which gives the solid angle of the sky surveyed to the sensitivity R. Integral versions of these curves are given for each filter in Fig. 6. A differential version of the coverage function for the Lexan/B filter is shown in Fig. 7.

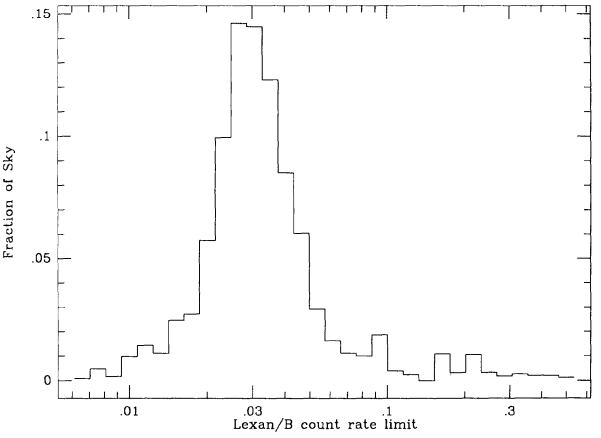

FIG. 7. Differential coverage function for the Lexan/B band, in bins of 0.075 dex.

The sky coverage function for the Lexan/B filter was checked by plotting the distribution of count rates for sources with low SNR. The measured count rates were normalized by $6/(\Delta S)^{1/2}$ and each source was given an equal fraction of the sky. The two distributions match reasonably well (Fig. 8).

5.2 Source Counts

One may construct the integral source counts for each filter by forming

$$N(>R)=\sum_{R_i>R}\frac{1}{\Omega(R_i)}. \quad (3)$$

This curve is computed for all sources satisfying the significance criterion ($\Delta S>36$) and is shown in Fig. 9 for the Lexan/B band only and in Fig. 10 for all filters. The number count curve reproduced from Pounds *et al.* (1993) is shown for comparison in Fig. 9.[8] These two distributions can be compared by shifting the WFC curve by a factor of 2.1 to account for the different effective areas of the two instruments (the *EUVE* filter has the larger effective area). This factor was derived by comparing the WFC and BSL count rates for white dwarfs in both catalogues and appears independent of average count rate. The shifted WFC curve is also presented in Fig. 9 and shows substantial deviations (>20%) from the corresponding *EUVE* curve at count rates below about 0.05 counts/s. This deviation could be due to incompleteness in the *EUVE* BSL, but it is not likely to be caused by a defect in the estimate of the sky coverage. Because the remaining three bands have never been observed elsewhere, it is very difficult to estimate completeness from external data.

[8]The sky coverage function was estimated graphically from Fig. 7(a) of Pounds *et al.* (1993).

© American Astronomical Society • Provided by the NASA Astrophysics Data System

1994AJ....107..751M

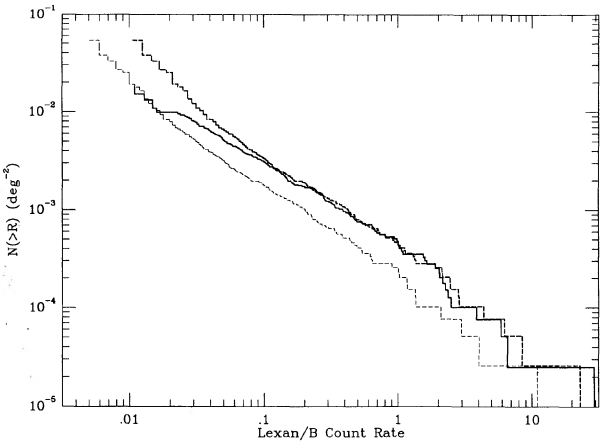

FIG. 9. Number count distribution computed using Eq. (3) for the Lexan/B bands of *EUVE* (bold solid line) and WFC (thin dashed line) surveys. Because the instruments have different effective areas, the WFC curve has been shifted upward by a factor of 2.1 (determined from count rates of mutually observed white dwarfs) for comparison. (bold dashed line). The agreement between the shifted WFC and the *EUVE* curves is very good for count rates greater than 0.05 counts s^{-1}.

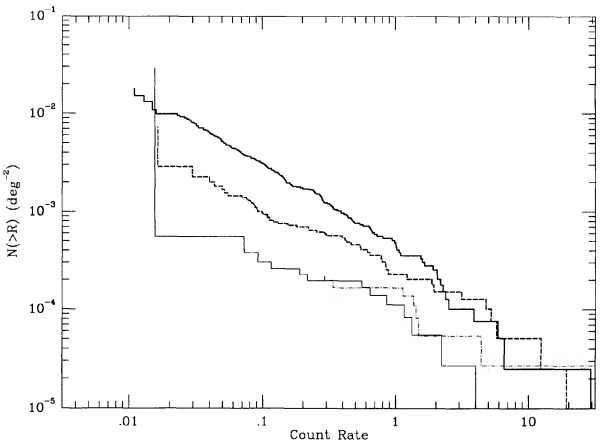

FIG. 10. Same as in Fig. 9 for all of the *EUVE* scanner wavelength bandpasses. Lexan/B: bold solid line; Al/C: bold dashed line; Dagwood: dashed-dotted line; tin: solid thin line.

A likelihood method that uses the information in the many count rate limits from Fig. 6 was used to estimate the value of a single power law fit to the data (see Marshall 1985). We find $N(>R)=19.3R^{-\alpha}$ sources per sky, where $\alpha=0.80\pm0.05$. These values are consistent with those of Pounds *et al.* (1993), after applying the ratio of 2.1 to convert the WFC count rate, *C*1, to *EUVE* count rate, *R*.

6. CONCLUSIONS

We have presented the list of 356 bright sources detected with the *EUVE* satellite during the in-orbit calibration phase of the mission and during the all-sky and deep surveys. More than 100 sources have been observed in the wavelength interval between 200 and 800 Å. For each source we have listed the maximum likelihood *EUVE* position and the *EUVE* count rate. For 341 sources we propose a possible optical identification and visual magnitudes. Fifteen EUV sources do not have any plausible optical counterpart, and follow-up spectroscopy and photometry are in progress to find the new optical identifications and to confirm the others. The two largest classes of source detected at the EUV wavelength are the late-type and white dwarf stars.

The authors would like to thank the entire *EUVE* team at the University of California, Berkeley; in particular we acknowledge the critical roles of M. Abbott, D. Biroscak, J. Drake, J. Dupuis, A. Hopkins, W. Marchant, M. Lampton, R. Lieu, and S. Vennes. We thank NASA's Goddard Space Flight Center (GSFC), which manages the *EUVE* project: the GSFC Project Manager, Paul Pashby; the Project Scientist, Dr. Yoji Kondo; the Deputy Project Scientist, Dr. Ronald Oliversen; the NASA Headquarters Program Scientist, Dr. Robert Stachnik; the Deputy Program Scientist, Dr. Derek Buzasi; the Program Manager, Dr. Guenter Riegler; and the GSFC Project Operations Director, Kevin Hartnett. We would also like to acknowledge the critical roles that Frank Martin, Charles Pellerin, and Ed Weiler have played in ensuring the success of *EUVE*. We acknowledge Andrea Frank's editorial assistance. This research is supported by NASA Contract Nos. NAS5-29298 and NAS5-30180.

REFERENCES

Antia, B. 1993, JBIS, 46, 337
Bowyer, S., Lieu, R., Lampton, M., Lewis, J., Wu, X., Drake, J. J., & Malina, R. F. 1993, ApJS (submitted)
Bowyer, S., Lieu, R., Lampton, M., & Sidher, S. D. 1993, Science (submitted)
Bowyer, S., & Malina, R. F. 1991, in Extreme Ultraviolet Astronomy, edited by R. F. Malina and S. Bowyer (Pergamon, New York), p. 397
Chakrabarti, S., Krasnopolsky, V., & Gladstone, G. R. 1993, BAAS, 25, 855
Christian, C., *et al.* 1993, ApJ, in preparation
Cruddace, R. G., Hasinger, G. R., & Schmitt, J. H. 1988, in Astronomy from Large Databases (ESO, Garching), p. 177
Cully, S., Siegmund, O. H. W., Vedder, P. W., & Vallerga, J. V. 1993, ApJ, 414, L49
Edelstein, J., Vedder, P. W., & Sirk, M. 1993, BAAS, 25, 863
Egret, D., Wenger, M., & Dubois, P. 1991, in Databases and On-line Data in Astronomy, edited by M. A. Albrecht and D. Egret (Kluwer, Dordrecht), p. 79
Finley, D., Jelinsky, P., Bowyer, S., & Malina, R. F. 1988, Appl. Opt., 27, 1476
Finley, D., Jelinsky, P., Dupuis, J., & Koester, D. 1993, ApJ, 417, 259
Gladstone, G. R., McDonald, J. S., Boyd, W. T., & Bowyer, S. 1993, BAAS, 25, 862
Helou, G., Madore, B. F., Schmitz, M., Bicay, M. D., Wu, X., & Bennett, J. 1991, in Databases and On-line Data in Astronomy, edited by M. A. Albrecht and D. Egret (Kluwer, Dordrecht), p. 89
Lewis, J. W. 1993, JBIS, 46, 346

© American Astronomical Society • Provided by the NASA Astrophysics Data System

1994AJ....107..751M

Lewis, J. W., Girouard, F. G., & McDonald, J. S. 1993, IEEE Trans. Softw. Eng., in preparation
Marshall, H. L. 1985, ApJ, 289, 457
Marshall, H. L., Carone, T., & Fruscione, A. 1993, ApJ, 414 L53
Moos, H. W., *et al.* 1993, BAAS, 25, 828
NASA Research Announcement No. 93-OSSA-02
Patterer, R. J., Vedder, P. W., Jelinsky, P., Brown, A., & Bowyer, S. 1993, ApJ, 414, L57
Pounds, K. A., *et al.* 1993, MNRAS, 260, 77
Siegmund, O. H. W., Lampton, M., Chakrabarti, S., Vallerga, J. V., Bowyer, S., & Malina, R. F. 1986, in Instrumentation in Astronomy VI, edited by D. L. Crawford, Proc. SPIE, 627, 660
Stringfellow, G., & Bowyer, S. 1993, in IAU Circular No. 5803, V1974 Cygni
Vallerga, J. V., Vedder, P. W., & Siegmund, O. H. W. 1992, in Multilayer and Grazing Incidence X-ray/EUV Optics for Astronomy and Projection Lithography, edited by R. B. Hoover and A. B. Walker, Jr., Proc. SPIE, 1742, 392
Vallerga, J. V., Vedder, P. W., & Welsh, B. Y. 1993, ApJ, 414, L65
Vedder, P. W., Patterer, R. J., Jelinsky, P., Brown, A., & Bowyer, S. 1993, ApJ, 414, L61
Vedder, P. W., Vallerga, J. V., Gibson, J., Stock, J., & Siegmund, O. H. W. 1992, in Multilayer and Grazing Incidence X-ray/EUV Optics for Astronomy and Projection Lithography, edited by R. B. Hoover and A. B. Walker Jr., Proc. SPIE, 1742, 486
Vennes, S., Dupuis, J., Rumph, T., Drake, J., Bowyer, S., Chayer, P., & Fontaine, G. 1993, ApJ, 410, L119
Warren, J., Vallerga, J. V., Mauche, C. W., Mukai, K., & Siegmund, O. H. W. 1993, ApJ, 414, L69
Welsh, B. Y., Vallerga, J. V., Jelinsky, P., Vedder, P. W., Bowyer, S., & Malina, R. F. 1990, Opt. Eng., 29, 752

© American Astronomical Society • Provided by the NASA Astrophysics Data System